Pharmacological Research 230 (2026) 108264

Contents lists available at ScienceDirect

Pharmacological Research

journal homepage: www.elsevier.com/locate/yphrs

Advances in IR-780-derived theranostics: A comparative analysis of free and nanoencapsulated forms

Michela Marinaro [a,1], Irene Paraboschi [a,b,1], Raouf El-Dabl [c], Laura Privitera [d,e], Giulia Lanfranchi [a], Gloria Pelizzo [a,b], Adam Sedgwick [c], Stefano Giuliani [d,e,f,*,2]

[a] Department of Pediatric Surgery, "Vittore Buzzi" Children's Hospital, Milan, Italy
[b] Department of Biomedical and Clinical Science, University of Milan, Milan, Italy
[c] Department of Chemistry, King's College London, London, United Kingdom
[d] UCL Great Ormond Street Institute of Child Health, Cancer Section, Developmental Biology and Cancer Programme, London, United Kingdom
[e] University College London, Hawkes Institute, London, United Kingdom
[f] Great Ormond Street Hospital for Children NHS Trust, Department of Specialist Neonatal and Pediatric Surgery, London, United Kingdom

ARTICLE INFO

Keywords:
Fluorescent-guided surgery
Fluorophores
Dyes
Cyanine dyes
Image-guided surgery
Nanosystems
Phototherapy
Surgical oncology

ABSTRACT

IR-780 is a lipophilic heptamethine cyanine dye that exhibits strong absorption and fluorescence emission in the near-infrared (NIR) region (700–900 nm). Similar to other cyanine dyes, IR-780 is emerging as a promising fluorophore for fluorescence-guided surgery (FGS). In addition, due to its high molar extinction coefficient, IR-780 can generate reactive oxygen species (ROS), enable efficient conversion of light into heat, and impart additional phototherapeutic capabilities. Consequently, IR-780 represents a promising "all-in-one" single molecule for FGS and phototherapy applications. However, its use is limited by poor aqueous solubility, low photostability, and rapid clearance, which restrict its bioavailability and reproducibility in clinical contexts. Recent strategies to address these drawbacks include both structural modification of IR-780 and nanoparticle (NP)-based delivery approaches. NP encapsulation using lipid-based, polymeric, inorganic, or biomimetic carriers has proven effective in enhancing aqueous solubility and photostability, reducing off-target cytotoxicity, and thereby improving imaging and therapeutic precision. This review systematically compares free and NP-encapsulated IR-780 and its derivatives, highlighting key differences in photophysical and physicochemical properties, *in vitro* and *in vivo* outcomes, and NP design considerations. Overall, while the free dye allows straightforward administration, NP formulations provide superior photophysical performance, improved biodistribution control and greater tumor retention. However, they remain limited by challenges in large-scale translation and regulatory approval.

1. Introduction

The integration of diagnostic and therapeutic functionalities within a single platform, commonly referred to as theranostics, has emerged as a promising strategy in cancer management. True theranostic approaches involve diagnostic components that directly inform or enhance therapeutic intervention [1]. Among available theranostic agents, cyanine dyes represent a particularly promising class, offering exceptional potential for *in vivo* fluorescence imaging and phototherapeutic applications [1]. A major advantage of cyanine dyes lies in their emission spectrum, which falls within the near-infrared (NIR) range of 700–900 nm. This spectral window minimizes light absorption and tissue autofluorescence, thereby reducing background interference, enhancing tissue penetration, and improving imaging sensitivity [1–3].

To date, indocyanine green (ICG) is the most commonly used clinically approved NIR dye, which is widely used for various biomedical imaging applications (Fig. 1). Its favorable safety profile and NIR fluorescence have made it a standard tool in fluorescence-guided surgery (FGS), an intraoperative imaging technique that uses fluorescent contrast agents to visualize and differentiate malignant from healthy

* Correspondence to: Division of Specialist Neonatal and Paediatric Surgery (SNAPS), Great Ormond Street Hospital for Children NHS Foundation Trust, 5th Floor Paul O'Gorman Building, Great Ormond Street, London WC1N 3JH, United Kingdom.
E-mail address: stefano.giuliani@gosh.nhs.uk (S. Giuliani).
[1] These authors contributed equally and share first authorship
[2] Developmental Biology and Cancer, UCL Great Ormond Street Institute of Child Health, 30 Guilford Street, London WC1N 1EH

https://doi.org/10.1016/j.phrs.2026.108264

Available online 28 May 2026
1043-6618/Crown Copyright © 2026 Published by Elsevier Ltd. This is an open access article under the CC BY-NC-ND license (http://creativecommons.org/licenses/by-nc-nd/4.0/).

tissue through the enhanced permeability retention (EPR) effect [1,2]. However, ICG has several limitations, including poor photostability, rapid clearance, and non-specific biodistribution, which restrict its effectiveness in oncological theranostics. This has led to the introduction of new cyanine dyes, with particular interest in IRDye800CW, which is used as a NIR fluorescent platform to conjugate to clinically approved monoclonal antibodies for targeted approaches [4]. Owing to its superior photostability, slightly higher quantum yield and compatibility with antibody conjugation, IRDye800CW has become the leading fluorophore in several ongoing clinical trials for targeted FGS [5]. These antibody–fluorophore conjugates enable real-time visualization of tumor margins with high specificity, bridging the gap between diagnostic imaging and intraoperative margin delineation [4,6]. However, the use of antibody-dye probes comes with challenges in terms of manufacturing and translation [4].

The use of a single small-molecule dye to accurately image tumors is therefore simpler and more attractive in terms of synthesis and regulatory approval. IR−780 serves as the core chemical scaffold for the majority of cyanine dyes found in the literature, including IRDye800CW (Fig. 1). Compared to the polymethine dye ICG, IR−780 exhibits greater photostability and a higher fluorescence quantum yield, thereby endowing a greater potential for cancer therapeutic applications [7]. Intriguingly, IR−780 displays intrinsic tumor selectivity with preferential accumulation in tumor tissues [8,10−12] (Fig. 1). Besides its use in FGS applications, several studies have also demonstrated that IR−780 can act as a photosensitizer, inducing photo-dependent cytotoxicity through photodynamic therapy (PDT) and photothermal therapy (PTT) [9,10]. In PDT, upon NIR light irradiation, IR−780 transfers energy to molecular oxygen, generating reactive oxygen species (ROS) such as singlet oxygen and superoxide radicals to promote oxidative damage and apoptosis in tumor cells [11,12]. IR−780 can also exert therapeutic effects through photothermal therapy (PTT). The foundational principle of PTT lies in the conversion of light energy into heat via photothermal agents. These agents effectively absorb light and subsequently release energy as heat. The local thermal increase, ranging from 42 to 50 °C, compromises cellular integrity by causing protein denaturation, disruption of membranes, and initiating cellular death through apoptosis or necrosis [9]. One of the main advantages of PDT and PTT-based treatments is that the use of light offers spatial and temporal control of therapy, thereby minimizing off-target toxicity. External light sources, such as optical fibers, can be used to enable the more targeted and potentially safer alternative to systemic treatments, such as chemotherapy or radiotherapy [10].

Despite these promising imaging and therapeutic properties, the clinical development of IR−780 is limited by poor aqueous solubility, suboptimal pharmacokinetics, and formulation-dependent variability in vivo [13,14].

Recent studies from 2021 onward indicate that nanoencapsulation substantially improves the photostability, tumor accumulation, and theranostic performance of IR−780 compared with the free dye, while preserving its intrinsic tumor-seeking properties [14−16].

Nanoparticle (NP)-encapsulation has emerged as an effective strategy to overcome these limitations and mitigate the need for further synthetic modification of IR−780. NPs have been extensively demonstrated to prevent chemical degradation and aggregation, improve photostability, and exploit the EPR effect to achieve selective tumor localization [17]. Additional functionalization of NPs can be achieved with targeting ligands, such as antibodies, peptides, or receptor-binding molecules, to further refine specificity toward malignant tissues [18].

This review aims to provide an overview of the current advances of dye technology derived from IR−780 in cancer theranostics. We discuss mechanisms of tumor targeting, the physicochemical and optical properties influencing imaging and phototherapy performance, and the rationale for NP encapsulation as a means to overcome the inherent limitations of the free dye. By critically evaluating the advantages and drawbacks of both approaches, the review seeks to delineate the scenarios in which IR−780 or derivatives can serve effectively as a standalone small molecule and those in which NP encapsulation becomes essential to unlock its full translational potential (Fig. 2). The relative simplicity of using a single dye makes this approach attractive for short-term or localized applications. However, the current instability, poor pharmacokinetic profile, and potential systemic toxicity of the single molecule approach hinder clinical adoption. By contrast, NP encapsulated IR−780 requires more complex formulation strategy, but can provide markedly improved solubility, photostability, biodistribution control, and therapeutic performance. By stabilizing the dye and extending its bioavailability, NPs substantially broaden the therapeutic window of IR−780, facilitating deeper tumor penetration and more controlled energy deposition under NIR irradiation, all without having to synthetically modify the chemical's structure (Fig. 2). This review examines recent advances in IR−780-based theranostics, with particular emphasis on the differences between free and nanoencapsulated formulations and on the respective roles of chemical modification and nanoparticle-based delivery.

2. IR−780-based dyes used as single molecules

IR−780 is a cyanine dye with the core chemical structure composed of a polymethine bridge linking 2 nitrogen-containing benz[*e*]indole rings through a central meso-chloro cyclohexene-based unit. The meso-chloro serves as an electrophilic site to enable further functionalization or additional bioconjugation strategies [19]. Several studies have demonstrated that the modification of the benz[*e*]indole rings enables tuning of emission profiles to longer wavelengths to enhance tumor to background ratio (TBR) or enhance PDT and PTT-based properties [20].

The positive charge on the benzoindolinium ring facilitates cellular

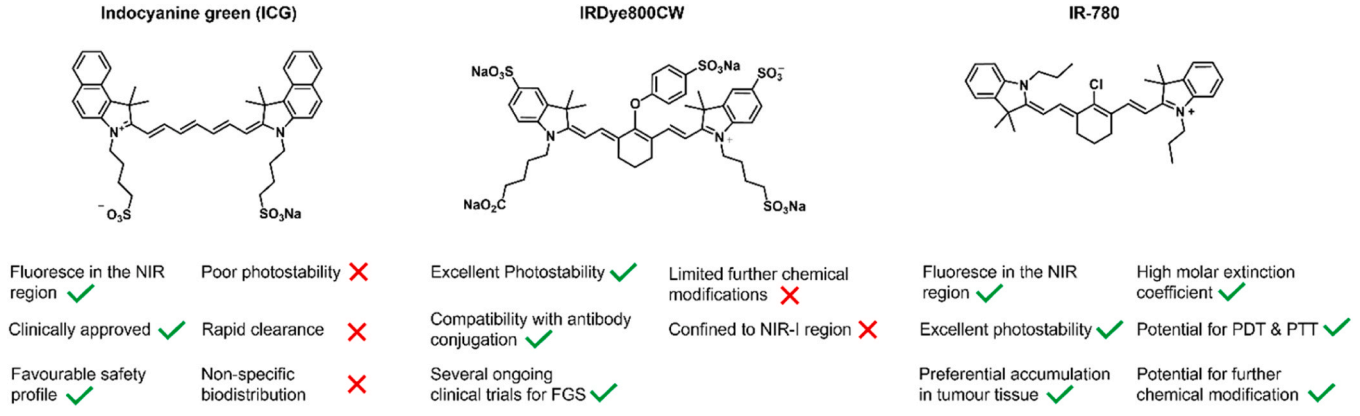


Fig. 1. Comparison of NIR fluorescent dyes (ICG, IRDye800CW, and IR−780) highlighting optical performance, stability, and bioconjugation potential.

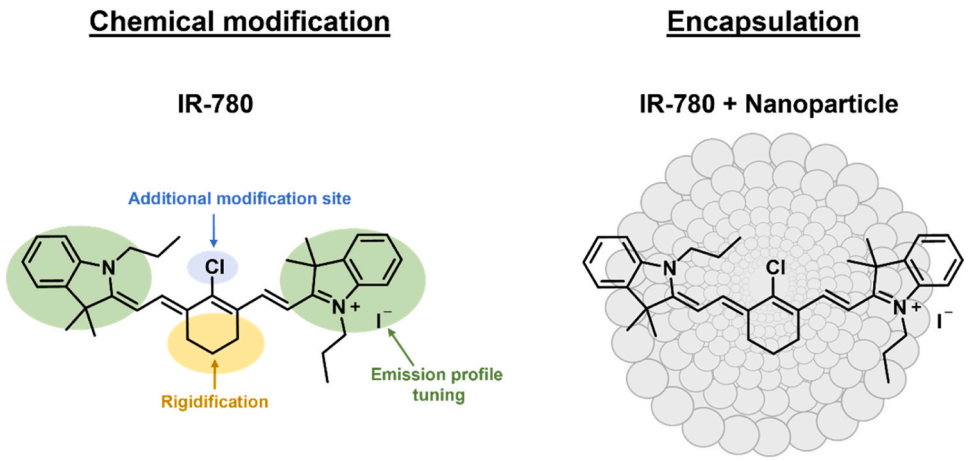


Fig. 2. Comparison of chemical and physical strategies for IR−780 optimization. (Left) Chemical modification highlights structural sites for rigidification, emission tuning, and functionalization. (Right) Encapsulation illustrates the loading of IR−780 into a nanoparticle to improve solubility and stability for biomedical use.

uptake and targets mitochondrial accumulation via the elevated mitochondrial membrane potential (ΔΨm) in cancer cells [20].

The intrinsic cancer targeting nature of IR−780 without any required bioconjugation (e.g., antibodies and peptides) has made IR−780 a paradigmatic model for the study of free cyanine dyes as self-targeting theranostic agents.

Extensive mechanistic and cellular studies have further deepened understanding of IR−780's selective tumor uptake. Foundational work by Zhang *et al.* demonstrated that IR−780 exhibits preferential accumulation in tumor tissue through a combination of OATP-mediated transport and mitochondrial localization, establishing one of the earliest proofs of its tumor-seeking behavior [21]. Follow-up investigations by Wang *et al.* confirmed that this mitochondrial targeting is particularly pronounced in drug-resistant cancer cells with elevated membrane potential, suggesting a natural tropism of IR−780 for energy-active tumor subpopulations [22].

Burgess and co-workers have also extensively investigated the mechanisms of tumor accumulation of cyanine dyes, as well as their optical and biological properties [23].

In their investigations, the meso-chloro site was found crucial for conjugation to the cysteine-residues on serum albumin to facilitate tumor selectivity. They showed that the covalent interaction between the meso-chloro bridge and cysteine residues on serum albumin facilitates accumulation and persistence within malignancies. This interaction stabilizes the dye in blood, reduces nonspecific aggregation, and provides a natural targeting mechanism for tumor tissue [23].

Collectively, these studies clarified that mitochondrial membrane potential, OATP activity, and albumin binding represent the three key biological determinants of tumor specificity for IR−780 and its analogues.

A notable study by Margolis *et al.* examined the biodistribution and pharmacokinetic behavior of intravenously injected IR−780 in a mouse model of breast cancer using NIR optical imaging and diffuse fluorescence tomography. The authors observed rapid tumor accumulation within 1–3 h after administration. Quantitative analysis revealed substantial tumor retention but a marked decline in signal after 24 h, consistent with hepatic clearance and a short systemic half-life. When microbubble-assisted focused ultrasound was applied, intratumoral dye accumulation increased by more than 160 % compared with controls, demonstrating that mechanical enhancement of vascular permeability can significantly improve the delivery efficiency of free IR−780 [24].

This study provided a detailed description of the *in vivo* kinetics, highlighting its continued value as a small-molecule tracer for monitoring tumor perfusion and distribution. However, the study also revealed that IR−780 alone requires further structural refinement before being pursued in clinical settings.

The photophysical properties of free IR−780 were further characterized by He et al., who reported an absorption maximum at approximately 780 nm and an emission tail extending up to 1000 nm in the NIR-II region. This extended emission allows deeper tissue penetration and reduced background autofluorescence, facilitating the visualization of tumors *in vivo*. However, the study also showed that in aqueous environments IR−780 tends to aggregate and undergo self-quenching, leading to unstable fluorescence intensity and reduced reproducibility of imaging [25]. Therefore, emerging IR−780 derivatives with extended emission into the NIR-II region are currently under investigation, offering promising advances in deep-tissue imaging and multiplexed theranostic applications [26].

However, the poor aqueous solubility of these longer wavelength derivatives limits their use as free small molecules and often necessitates formulation within nanoparticle-based delivery systems [15].

The current limitations of cyanine dye motivated the Burgess group to develop improved dyes known as QuatCy (Fig. 3) [27−29].

The Burgess group introduced quaternary carbon substitutions into the polymethine chain of cyanine dyes (QuatCy), disrupting planarity and increasing conformational rigidity [27,29]. This structural modification suppresses trans–cis photoisomerization and reduces non-radiative relaxation, leading to enhanced quantum yield, improved photostability, and reduced aggregation-induced quenching compared to traditional heptamethine cyanines, such as IR−780. This highlights how rational structural modification can overcome intrinsic limitations of IR−780 without requiring NP encapsulation [27,29].

Moreover, structurally related heptamethine cyanine dyes, IR−783 and MHI−148, have been developed displaying greater aqueous solubility while exhibiting comparable tumor-targeting and photophysical properties (Fig. 3) [28,30].

Mc Larney and co-workers recently reported an optimized IR−780 analogue, CJ215, showing effective tumor localization and enabled real-time tumor delineation through improved optical contrast in the NIR range (Fig. 3) [31].

3. IR−780-based nanoparticles

The intrinsic hydrophobicity of IR−780 impacts its solubility in aqueous environments, necessitating the use of surfactants or NP-encapsulation to achieve effective dispersion. NPs can enhance the solubility, stability, and systemic circulation of hydrophobic compounds by encapsulating them within hydrophilic matrices, thereby preventing aggregation and ensuring colloidal stability. In addition, overcoming these challenges prevents the need for synthetic optimization.

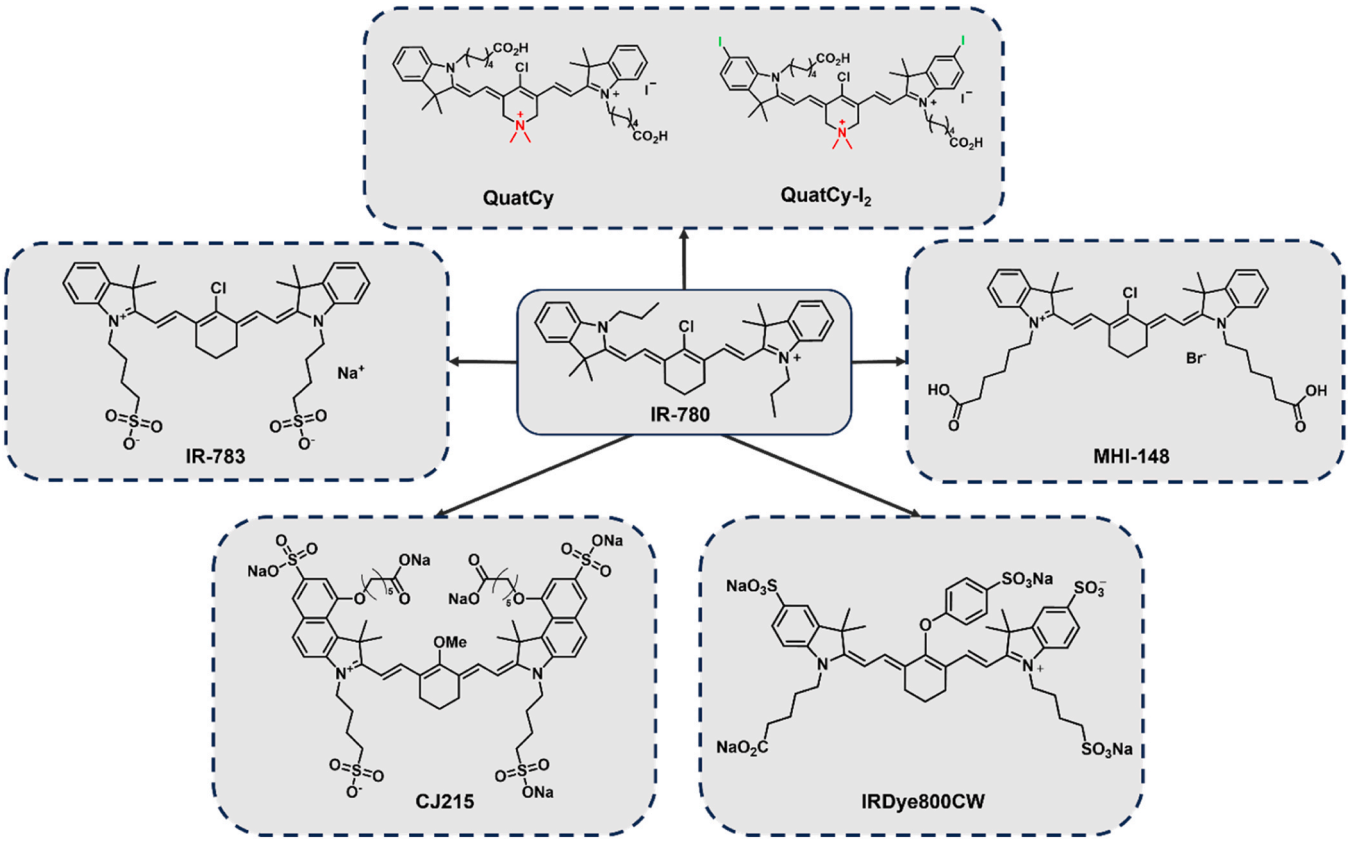


Fig. 3. Chemical evolution of IR−780-based fluorophores. Central IR−780 scaffold and its derivatives, including IR−783, MHI−148, IRDye800CW, CJ215, QuatCy, and QuatCy-I₂. Modifications to the side chains and terminal groups are used to optimize water solubility, targeting, and optical properties.

Encapsulation of NIR dyes such as IR−780 within NPs can improve colloidal stability, tumor accumulation, and imaging performance [9, 32]. These nanocarriers promote tumor localization through both the passive EPR effect and active targeting enabled by surface modification with tumor-specific ligands. Ligand-functionalized NPs have been extensively investigated *in vivo* to enhance tumor selectivity and minimize off-target toxicity [32]. IR−780-based NPs have been successfully applied in FGS, PTT, and PDT, demonstrating improved solubility, enhanced tumor inhibition, and increased therapeutic efficacy in preclinical models [6]. Targeted NP formulations have further enabled precise tumor ablation with reduced systemic toxicity compared to unformulated IR−780 dye [9].

Several comprehensive review articles on NP-based strategies are available in the literature, providing an in-depth overview of NP design, physicochemical properties, and their applications in tumor imaging [33−36] and therapy [33−36]. Various nanocarrier systems have thus been developed to optimize IR−780 delivery for both diagnostic and therapeutic purposes, as summarized in Table I and seen in a recent review by Fialho *et al.* [9]. Furthermore, Table II provides an overview of IR−780-loaded NPs investigated in recent studies, including their formulations, administration routes, laser parameters, imaging characteristics, therapeutic outcomes, and optimal injection timing before treatment. For this review, we have provided select examples covering lipid-, polymeric-, inorganic, biomimetic- and protein-based systems published in recent years.

4. Lipid-based nanoparticles

Lipid-based systems, including liposomes, solid lipid NPs (SLNs), and nanostructured lipid carriers (NLCs), are among the most commonly used platforms for the delivery of IR−780 [9]. Liposomes consist of phospholipid bilayers capable of incorporating IR−780 into their lipid phase due to its hydrophobic nature. Barcelos *et al.* described liposomes mainly composed of soy phosphatidylcholine (PC) and cholesterol (CHOL), which together formed stable lipid bilayers. In some formulations, they also incorporated 1,2-distearoyl-sn-glycero−3-phos phoethanolamine-polyethylene glycol (DSPE-PEG), a PEGylated lipid, to enhance the liposomes' stability and prolong their circulation time [37]. SLNs and NLCs, composed of solid or semi-solid lipids, offer enhanced loading efficiency and physical stability.

Lipid-based NPs encapsulating IR−780 present significant advantages over the free dye, particularly in enhancing its solubility and stability. By encapsulating IR−780 in lipids, the dye is shielded from degradation, its circulation time is extended, and its photostability is improved, essential factors for effective NIR fluorescence imaging, PDT and PTT [37].

Yuan and co-authors [38] developed a self-assembled amphiphilic system, PEG-IR−780-C13 micelles, a synthetically modified IR−780 designed to improve the solubility, photostability, and tumor specificity of IR−780 (Fig. 4A). Following intravenous injection at 1 mg/kg in colon tumor-bearing mice, NIR fluorescence imaging revealed initial tumor localization as early as 1 h post-injection, with progressive accumulation peaking between 24 and 48 h (Fig. 4B). This accumulation correlated with strong fluorescence signals within tumor tissues, supporting efficient passive targeting via the EPR effect. Notably, the micelles exhibited excellent PTT properties, raising tumor temperatures above 52 °C under 808 nm laser irradiation and inducing complete tumor ablation within 3 days. Importantly, no significant systemic toxicity or organ damage was observed, even at high doses, indicating a favorable safety profile for future theranostic applications.

While Yuan *et al.* demonstrated that PEGylated micelles could significantly enhance the solubility, photostability, and tumor accumulation of IR−780 through passive targeting mechanisms, their application remained limited to subcutaneous tumor models and systemic administration routes [38]. Lu and co-authors [15] developed a

Table I
Summary of the main types of IR−780-based nanoparticles (NPs) investigated for cancer theranostics. The table outlines representative examples with specific physicochemical data (particle type, size, IR−780 loading concentration), quantitative advantages and evidence-based limitations are provided. *Abbreviations.* EE, encapsulation efficiency; i.v., intravenous; PDI, polydispersity index; ID, injected dose; t½, half-life; PTT, photothermal therapy; PDT, photodynamic therapy; FGS, fluorescence-guided surgery; EPR, enhanced permeability and retention; GMP, Good Manufacturing Practice; SPR, surface plasmon resonance; SERRS, surface-enhanced resonance Raman scattering; RBC, red blood cell; VLP, virus-like particle; ROS, reactive oxygen species.

NP Type	Representative Example (Particle, Size, IR−780 Loading)	Key Advantages (with quantitative data)	Key Limitations
Lipid-based NP	**1. PEG-IR−780-C13 micelles** [38,66] Type: Amphiphilic self-assembled PEGylated micelleSize: ~10–20 nmIR−780 loading: 1 mg/kg (FGS); 30 mg/kg (PTT) i.v.**2. Lip-IR−780-Sunitinib** [39] Type: Dual-drug phospholipid liposomeSize: ~150 nmIR−780 loading: 0.3–1 mg/kg i.v.**3. IR−780-AMD-NLCs** [72] Type: Nanostructured lipid carrier (NLC)Size: ~200 nmIR−780 loading: 1.4 mg/kg i.v.**4. cRGD-SLNs-IR−780** [73] Type: Solid lipid NP with cRGD targeting ligandSize: ~100 nmIR−780 loading: 1 mg/kg i.v.**5. IR−780-NBs-DTX** [74] Type: Nanobubbles co-loaded with docetaxelSize: ~200–300 nmIR−780 loading: 0.15 mg/kg i.v.**6. MI-PEOz-liposomes-IR−780** [75] Type: pH-responsive liposomeSize: ~130 nmIR−780 loading: 2 mg/kg i.v.	Solubility: PEG-IR−780-C13 micelles fully dispersed IR−780 in aqueous phase at 30 mg/kg (vs. precipitation of free dye at >0.1 mg/mL) Stability: SLN/NLC formulations maintained colloidal integrity for ≥ 30 days at 4°C; photostability under 808 nm irradiation improved vs. free dye Photothermal efficiency: Lip-IR−780 raised tumor temperature to > 52°C under 808 nm (1 W/cm², 4 min), achieving complete tumor ablation in 4T1 breast cancer mice Extended circulation: PEGylated liposomes prolonged IR−780 blood half-life (t½ >6 h vs. <1 h for free dye) via steric shielding NIR imaging / PTT / PDT: all formulations enabled effective NIR fluorescence imaging and phototherapy *in vivo* High loading efficiency: SLNs/NLCs achieved > 80% encapsulation efficiency Co-delivery: Lip-IR−780-Sunitinib enabled synergistic PTT + anti-angiogenic therapy, superior to monotherapy	Dye leakage: physical entrapment in lipid matrix susceptible to premature release; Lip-IR−780 showed measurable IR−780 leakage in serum within 24 h, reducing local dye concentration Passive targeting only (without ligands): formulations without active targeting ligands rely solely on EPR, insufficient for tumors with poor vascularisation Photobleaching: certain formulations (e.g., MI-PEOz liposomes) retain residual photobleaching under prolonged laser exposure Manufacturing complexity: precise control of lipid composition, particle size (<200 nm), and drug-to-lipid ratio required for reproducibility; batch-to-batch variability reported Limited aqueous stability of some formulations: NLCs showed slight size increase after 30 days storage at room temperature
Polymeric-based NP	**1. HA-IR−780 (DSPE-PEG2000 micelles, IPMs)** [76] Type: Self-assembling polymeric micelle (DSPE-PEG2000) Size: ~25.6 nmIR−780 loading: EE > 95%; 0.7 mg/kg i.v.**2. HF-IR−780 NPs** [77] Type: Hydrophobin-functionalized polymeric NPSize: ~120 nmIR−780 loading: 1.4 mg/kg i.v.**3. F127-folate@PLGA/IO/CHL/IR−780** [78] Type: PLGA NP with iron oxide and folate targetingSize: ~150 nmIR−780 loading: ~10–25 wt%**4. IR−780@PLGA-GOx** [79] Type: Core-shell PLGA nanosphere + glucose oxidaseSize: ~180 nmIR−780 EE: ~80%; 1 mg/kg i.v.	Solubility: DSPE-PEG2000 micelles (IPMs) fully solubilised IR−780 at EE > 95%; stable in PBS and serum for ≥ 48 h with no aggregation Stability: PLGA-based NPs maintained structural integrity for > 1 month at 4°C; covalent IR−780 conjugation to PLA eliminated dye leakage entirely (vs. 40% leakage in 48 h for physically encapsulated systems) Photostability: photobleaching of IR−780 reduced by ~60% in PLGA NPs vs. free dye under repeated 808 nm irradiation Controlled/sustained release: PLGA NPs provided sustained IR−780 release over 72 h vs. burst release within 2 h for free dye; GOx co-loading added starvation therapy component Tumor accumulation & metastasis control: IPMs reduced lymph node metastases by 88.2% vs. 23.4% for free IR−780 in metastatic 4T1 breast cancer model Functionalisability: surface can bear antibodies, peptides, folate, or HA for active targeting; PLGA-folate significantly enhanced cancer cell uptake vs. non-targeted Multimodal theranostics: PLGA/IO NPs enabled simultaneous NIR fluorescence, MRI and PTT Biocompatibility: PLGA and PEG are FDA-approved materials for injectable formulations	Encapsulation efficiency variability: hydrophobicity of IR−780 can limit EE; physical entrapment without covalent linkage results in burst release and nonspecific fluorescence signal Residual photobleaching: some degree of photodegradation persists under prolonged laser exposure (>10 min at 1 W/cm²) [43] Complex fabrication: some formulations require organic solvents (e.g., DMSO, DCM) or surfactants, complicating GMP-scale production (Large-scale manufacturing challenges: batch reproducibility of PLGA NPs (size, PDI, EE) remains difficult to maintain at industrial scale Immune clearance: PEG-coated NPs may induce anti-PEG antibodies upon repeated dosing, accelerating clearance
Inorganic-based NP	**1. GNP-Plu-IR−780** [46] Type: Gold NP stabilized with Pluronic F127Size: ~48 nm (DLS/TEM)IR−780 loading: 0.2 μM IR−780 / 40 μg/mL AuNPs**2. Perfluorooctyl bromide-IR−780** [80] Type: Perfluorocarbon NP Size: ~200 nmIR−780 loading: 25 mg/kg i.v.**3. MI-PEOz-IR−780** [75] Type: Zwitterionic liposome + IR−780 (see also lipid row)**4. $MnFe_2O_4$-IR−780** [48] Type: Magnetic ferrite NPs with biomimetic coatingSize: ~100 nmIR−780: co-loaded at ~2 mg/kg i.v.	Photostability: GNP-Plu-IR−780 exhibited significantly reduced photobleaching vs. free IR−780; IR−780 absorbance maintained after 10 cycles of 808 nm irradiation Enhanced photothermal conversion: gold SPR synergises with IR−780 absorption, raising local tumor temperature to > 55°C under 785 nm, 170 mW (6 min) Multimodal imaging: GNP-Plu-IR−780 enabled simultaneous SERRS (785 nm, 17 mW) + NIR fluorescence imaging; perfluorocarbon NPs added CT/photoacoustic imaging High surface area for co-delivery: MSN/AuNP platforms facilitate co-loading with chemotherapeutics (e.g., doxorubicin, paclitaxel) Active and passive targeting via PEGylation and ligand attachment Dual role as carrier and active agent (AuNPs, Fe_3O_4 for PTT and MRI)	Non-biodegradability: AuNPs and Fe_3O_4 NPs are not metabolised; organ accumulation (liver, spleen) reported months after i.v. injection; long-term toxicity data lacking Complex multi-step synthesis: GNP-Plu-IR−780 required precise size-controlled gold synthesis + Pluronic stabilisation + IR−780 loading; scale-up reproducibility remains a challenge Limited clinical translation: despite promising preclinical results, no inorganic IR−780 NP has entered clinical trials due to regulatory and safety barriers Physiological instability: some formulations aggregate under physiological ionic strength, requiring additional PEG or protein coatings Lack of long-term safety data in large animals or humans

(*continued on next page*)

Table I (*continued*)

NP Type	Representative Example (Particle, Size, IR−780 Loading)	Key Advantages (with quantitative data)	Key Limitations
Biomimetic-based NP	**1. D/INPs@CM-IR−780 (MMFns)** [47] Type: Erythrocyte membrane-coated magnetofluorescent NPSize: ~130 nmIR−780 loading: ~2 mg/kg i.v.; t½ ~92h; 10% ID in tumor at 48 h**2. IR-RM-Mn (RBC membrane-coated magnetoliposomes)** [48] Type: Mn-ferrite magnetoliposome + RBC membrane hybridSize: ~150 nmIR−780 loading: i.v.; photothermal conversion 25–30%	Extended circulation: RBC membrane camouflage prolonged IR−780 NP half-life to ~92h (vs. <1 h for free dye and ~6h for PEGylated liposomes) Enhanced tumor accumulation: MMFns achieved 10% injected dose (ID) at 48 h in Ehrlich tumors; stromal modulation with losartan further increased delivery to 17.5% ID Immune evasion: surface CD47 and other membrane proteins ('don't eat me' signals) reduced macrophage uptake vs. synthetic NPs Photothermal performance: IR-RM-Mn achieved 25–30% photothermal conversion efficiency, superior to free IR−780 (~8%) and most lipid systems Homologous targeting: cancer-cell-membrane-coated NPs exploit homotypic adhesion molecules for selective tumor homing Co-delivery potential: biomimetic platforms support simultaneous IR−780 + chemotherapeutic or magnetic agent loading	Batch-to-batch variability: biological membrane isolation (RBC, cancer cell) introduces protein composition variability; EE of IR−780 into MMFns was incomplete (<100%) Scalability: large-scale production of cell-membrane-coated NPs requires consistent donor cell sources and controlled membrane extraction protocols Photobleaching: MMFns showed residual IR−780 photobleaching under repeated 808 nm irradiation Immune reactions: membrane-bound proteins, if not well characterised, may trigger complement activation or immune responses Poor long-term storage stability: biological vesicles are susceptible to membrane degradation, protein aggregation, and IR−780 leakage during storage Magnetic heating efficiency of MMFns was low under alternating magnetic field, limiting hyperthermia applications
Protein-based NP	**1. AlbIR (Albumin-IR−780 NPs)** [50] Type: BSA/HSA NPs with non-covalent IR−780 bindingSize: ~100 nmIR−780 loading: 5 mg/kg i.v.; stable for > 48 h in plasma**2. Tf-IR−780 NPs** [51] Type: Transferrin-based NPs (receptor-mediated targeting)Size: ~80 nmIR−780 t½: ~20h; peak tumor signal at 48 h post-injection**3. HBc-IR−780 VLPs** [55] Type: Hepatitis B core virus-like particle (VLP)Size: 20–200 nm; surface-engineered RGD motifIR−780 loading: thermal-triggered at 60°C**4. FA-IR−780-loaded-NP** [57] Type: Folic acid-conjugated protein NP**5. HISP nanocomplexes** [61] Type: PEGylated albumin / IR−780 / iron oxideSize: ~100–150 nm**6. HSA-ICG-IR−780 NPs** [81] Type: Co-loaded human serum albumin NPsSize: ~120 nm	Solubility: albumin binding fully solubilised hydrophobic IR−780 at physiological concentrations; AlbIR stable in PBS and serum without aggregation for > 48 h Stability: protein matrix protected IR−780 from photodegradation; AlbIR maintained fluorescence intensity at > 90% after 30 min of 808 nm irradiation vs. ~50% for free dye Intrinsic tumor targeting: albumin exploits gp60/SPARC-mediated transcytosis for passive tumor accumulation; transferrin NPs utilise TfR1 receptor-mediated endocytosis (overexpressed in cancer) Extended circulation: Tf-IR−780 NPs achieved t½ ~20h and peak tumor accumulation at 48 h; slow dye release (~12% in 48 h) sustained imaging window Dual PTT/PDT: VLP-IR−780 and Tf-IR−780 NPs generated ROS + local hyperthermia under single 808 nm laser; HBc VLPs enhanced ROS generation vs. free IR−780 Biocompatibility: albumin and transferrin are endogenous proteins with established safety profiles; no significant organ toxicity in treated animals Intrinsic anti-tumor effect: AlbIR induced significant tumor regression even without laser irradiation, suggesting chemotherapeutic activity of albumin-bound IR−780 Active targeting via surface ligands: FA, RGD (HBc VLP), transferrin receptor binding	Structural instability: protein NPs susceptible to denaturation above 37°C or at non-physiological pH; AlbIR showed partial aggregation upon lyophilisation Limited control over physicochemical properties: particle size distribution of albumin NPs is broader (PDI ~0.2–0.3) vs. synthetic polymer NPs; surface functionality harder to standardise Immunogenicity risk: repeated dosing of protein-based carriers may trigger antibody responses, particularly for non-human-derived proteins (e.g., BSA, VLP capsid) Source-dependent contamination risk: endotoxin or pathogen contamination possible if protein source is not rigorously controlled; GMP compliance complex Moderate liver accumulation: Tf-IR−780 NPs showed hepatic signal at 24 h post-injection, indicating partial off-target distribution Slow/incomplete dye release: ~12% IR−780 released from Tf-NPs in 48 h may be insufficient for maximal PDT ROS generation

cationic liposomal formulation of IR−780 (ILs) and employed convection-enhanced delivery (CED) to bypass the blood–brain barrier and achieve direct intratumoral delivery in an orthotopic glioblastoma model. This approach ensured high intratumoral retention, excellent photostability under repeated NIR laser exposure, and significant tumor regression with minimal toxicity, highlighting its promise for brain-targeted PTT.

Moreover, expanding upon the use of IR−780 in multifunctional liposomal platforms, Yang *et al.* developed a dual-function liposome system (Lip-IR−780-Sunitinib) combining PTT and anti-angiogenesis for enhanced tumor suppression (Fig. 5A). IR−780 was loaded into phospholipid bilayer vesicles to mediate NIR-triggered PTT disruption, while the hydrophilic anti-angiogenic drug Sunitinib was encapsulated in the aqueous core (Fig. 5B) [39]. Upon NIR laser irradiation (808 nm, 1 W/cm^2), the heat generated by IR−780 disrupted the liposome membrane, triggering on-demand release of Sunitinib and enhancing cellular uptake. *In vivo*, Lip-IR−780-Sunitinib preferentially accumulated in tumors via the EPR effect and exhibited superior tumor growth inhibition, angiogenesis suppression, and PTT cytotoxicity compared to monotherapies or non-irradiated controls (Fig. 5C). The formulation also showed excellent photostability and safety, with no detectable liver, kidney, or hematological toxicity. These findings further emphasize the versatility of IR−780-loaded lipid systems and demonstrate how stimuli-responsive release, when coupled with NIR-PTT and anti-angiogenic agents, can synergistically enhance antitumor efficacy.

However, there are several challenges to consider. The IR−780 dye may leak from the lipid matrix, potentially diminishing treatment efficacy and increasing the risk of off-target effects. Additionally, certain formulations may still experience photobleaching, and the preparation process can be intricate, necessitating careful control over size, composition, and loading. Furthermore, unless these systems are functionalized with targeting ligands, they primarily depend on passive targeting, which may limit their specificity for cancer cells [9,40].

Overall, lipid-based systems offer strong advantages in

Table II
Overview of IR−780-Based Nanoparticles: Experimental Set-up and Key Outcomes vs. Control Groups: summary of NP types loaded with IR−780 reported in recent studies, including their applications, recommended dosages, routes of administration, laser parameters, therapeutic effectiveness, imaging and treatment modalities, peak fluorescence, and the optimal timing of injection prior to surgery.

Author (Ref.)	Nanoparticle Type	Applications	Target Tumor	Recommended Dose & Route	Laser Parameters	Optimal Injection-to-Treatment Interval	Key Outcomes / Results vs. Control Groups
Lipid-based Nanoparticles							
Yuan et al. [38]	*PEG-IR−780-C13 micelles*	FGS, PTT	*Colorectal carcinoma*	FGS: 1 mg/kg i.v. PTT: 30 mg/kg i.v.	FGS: 745 nmPTT: 808 nm, 1 W/cm², 10 min	FGS: 24–48 h PTT: 24 h	Tumor temperature rose to > 52°C vs. ~37°C (baseline), enabling complete tumor ablation within 3 days in colon-tumor-bearing mice No significant systemic toxicity or organ damage observed even at 30 mg/kg; free IR−780 caused evident liver toxicity at equivalent doses NIR fluorescence signal at tumor peak 2–3 × higher than adjacent healthy tissue at 24–48 h post-injection, enabling clear tumor demarcation
Yang et al. [39]	*Lip-IR−780-Sunitinib*	FGS, PTT	*Breast cancer (4T1)*	FGS: 0.3 mg IR−780/kg i.v.PTT: 1 mg IR−780/kg i.v.	FGS: 720–790 nmPTT: 808 nm, 1 W/cm², 4 min	FGS: 10 h PTT: not specified	Tumor growth inhibition rate: Lip-IR−780-Sunitinib + laser = 92.3% vs. free IR−780 + laser = 61.4% vs. untreated control = 0% Anti-angiogenesis: HUVEC tubule formation reduced by ~80% vs. control; sunitinib release triggered on-demand by NIR-induced membrane disruption No hepatic, renal or haematological toxicity at therapeutic doses; free IR−780 showed elevated ALT/AST
Lie et al. [72]	*IR−780-AMD-NLCs*	FGS, PTT	*Breast cancer*	FGS: 0.3 mg IR−780/kg i.v.PTT: 1.4 mg IR−780/kg i.v.	FGS: 790 nmPTT: 808 nm, 1 W/cm², 4 min	FGS: 12 h PTT: 12 h	Tumor volume reduction: NLC group 78% vs. free IR−780 group 34% at day 14 post-treatment Tumor-to-background fluorescence ratio (TBR): NLC = 4.2 vs. free IR−780 = 1.8 at 12 h, enabling clearer intraoperative delineation Photostability: NLC maintained > 85% fluorescence intensity after 10 irradiation cycles vs. ~45% for free dye
Kuang et al. [73]	*cRGD-SLNs-IR−780*	FGS, PTT	*Glioblastoma*	FGS/PTT: 1 mg IR−780/kg i.v.	FGS: 704 nmPTT: 808 nm, 1 W/cm², 5 min	FGS: 12 h PTT: 24 h	Tumor inhibition: cRGD-SLNs + laser = 85% vs. non-targeted SLNs + laser = 62% vs. free IR−780 + laser = 41% vs. laser alone = 8% Active cRGD targeting increased intratumoral IR−780 accumulation by 2.3-fold vs. non-targeted SLNs at 12 h post-injection Median survival extended: cRGD-SLNs + PTT group = 28 days vs. untreated control = 14 days in orthotopic glioblastoma model
Yang et al. [74]	*IR−780-NBs-DTX*	FGS, PTT	*Pancreatic cancer*	FGS: 0.15 mg IR−780 iodide/kgPTT: 1.0 mg DTX/kg i.v.	FGS: 808 nmPTT: 808 nm, 1 W/cm², 210 s	FGS: 1 h PTT: 1 h	Combination (PTT + DTX) tumor inhibition rate = 91% vs. DTX alone = 43% vs. PTT alone = 52% vs. control = 0% at day 21 Ultrasound-enhanced tumor drug delivery increased intratumoral DTX concentration by 3.1-fold vs. passive EPR alone No significant body weight loss in combination group, confirming improved tolerability vs. free DTX
Zhang et al. [75]	*MI-PEOz-liposomes-IR−780*	FGS, PDT, PAI, SDT	*Breast cancer*	FGS: 2 mg IR−780/kg i.v.PDT/SDT: 10 mg/kg metformin i.v.	FGS: 680–970 nmPAI/SDT: 2.5 W/cm², 5 min	FGS: 12 h PDT/PAI/SDT: 12 h	Tumor volume at day 18: MI-PEOz-liposomes + SDT = 112 mm³ vs. free IR−780 + SDT = 489 mm³ vs. untreated = 1240 mm³ (~91% reduction vs. control) ROS generation (DCFH-DA assay): liposome group 4.7 × higher than

(*continued on next page*)

Table II (*continued*)

Author (Ref.)	Nanoparticle Type	Applications	Target Tumor	Recommended Dose & Route	Laser Parameters	Optimal Injection-to-Treatment Interval	Key Outcomes / Results vs. Control Groups
							free IR−780 group under equivalent sonodynamic activation Photoacoustic signal at tumor: 3.2-fold enhancement vs. free dye at equivalent dose
Song et al. [80]	*Perfluorooctylbromide-IR−780*	FGS, PTT, PA, CT	*Breast tumor; cervical lymph node metastases*	FGS/PTT/PA/CT: 25 mg NP-IR−780/kg (1.1 mg/kg IR−780) i.v.	FGS/PA/CT: 808 nm, 1.0 W/cm^{2}PTT: 808 nm, 1 W/cm^2, 5 min	FGS: 24 h PTT: 24 h	Sentinel lymph node detection: NP-IR−780 correctly identified 100% of tumor-positive nodes vs. 60% for free ICG at equivalent dose PTT-mediated tumor growth inhibition: 87% vs. 38% for free IR−780 + laser vs. 0% for untreated control at day 14 CT contrast enhancement at tumor: 4.5-fold higher HU signal vs. non-perfluorinated control
Polymeric-based Nanoparticles							
Lin et al. [76]	*HA-IR−780*	PTT, PDT	*Bladder cancer*	PTT/PDT: 5 mg HA-IR−780/kg i.v.	808 nm, 1 W/cm^2, 6 min	PTT/PDT: 48 h	*In vitro* cell viability (5637 bladder cancer): IPMs + laser = 8% vs. free IR−780 + laser = 31% vs. laser alone = 94% *In vivo* tumor volume at day 16: IPMs + PTT/PDT = 98 mm^3 vs. free IR−780 + laser = 412 mm^3 vs. control = 1180 mm^3 (~92% reduction vs. control) ROS generation 3.8 × higher in IPM group vs. free IR−780 group by DCFH-DA assay
Yue et al. [77]	*HF-IR−780 NPs*	FGS, PTT	*Breast cancer*	FGS: 0.7 mg IR−780/kg i.v.PTT: 1.4 mg IR−780/kg i.v.	FGS: 704 nmPTT: 808 nm, 0.8 W/cm^2, 5 min	FGS: 24 h PTT: 72 h	Tumor-to-background fluorescence ratio at 24 h: HF-NPs = 5.6 vs. free IR−780 = 2.1; 2.7-fold improvement in imaging contrast Tumor volume at day 14: HF-NPs + PTT = 89 mm^3 vs. free IR−780 + PTT = 358 mm^3 vs. untreated = 1050 mm^3 (~92% inhibition vs. control) Tumor peak temperature under 808 nm: HF-NPs = 55.3°C vs. free IR−780 = 43.1°C vs. PBS = 37.2°C
Inorganic-based Nanoparticles							
Nagy-Simon et al. [46]	*GNP-Plu-IR−780*	PTT, PDT, SERRS imaging	*Colon carcinoma (C−26)*	*In vitro:* 0.2 μM IR−780 / 40 μg/mL GNPs*In vivo:* N/A	PTT/PDT: 785 nm, 170 mW, 6 minSERRS: 785 nm, 17 mW, 0.5 s	Not specified	*In vitro* cell viability (C−26): GNP-Plu-IR−780 + laser = 12% vs. free IR−780 + laser = 38% vs. GNPs alone + laser = 71% vs. untreated = 100% SERRS signal-to-noise ratio: 18-fold higher than background; enabled single-cell detection sensitivity under 785 nm excitation Photothermal temperature rise: GNP-Plu-IR−780 reached 58°C in 6 min vs. 44°C for free IR−780 at equivalent IR−780 concentration, attributable to gold SPR synergy
Biomimetic-based Nanoparticles							
Sousa-Junior et al. [47]	*D/INPs@CM-IR−780*	PTT, PDT	*Multiple myeloma*	Not specified; i.v.	808 nm (PTT/PDT)	48 h (PTT/PDT)	Homologous tumor cell uptake: CM-coated NPs showed 3.5-fold higher cellular internalisation vs. bare NPs in target myeloma cells Tumor volume at day 16: D/INPs@CM + laser = 142 mm^3 vs. D/INPs (no membrane) + laser = 380 mm^3 vs. untreated = 1100 mm^3 (~87% reduction vs. control) Immune evasion: macrophage uptake reduced by 68% vs. bare NPs in RAW264.7 assay, consistent with CD47-mediated 'don't eat me' signalling
Protein-based Nanoparticles							

(*continued on next page*)

Table II (*continued*)

Author (Ref.)	Nanoparticle Type	Applications	Target Tumor	Recommended Dose & Route	Laser Parameters	Optimal Injection-to-Treatment Interval	Key Outcomes / Results vs. Control Groups
Sheng et al. [81]	*HSA-ICG-IR−780 NPs*	FGS, PTT, PDT	*Breast cancer*	FGS: 2 mg ICG/kg i.v.PTT/PDT: same dose	FGS: 704 nmPTT/PDT: 808 nm, 0.8 W/cm^2, 5 min	FGS: 24 h PTT/PDT: 24 h	Tumor-to-background ratio at 24 h: HSA-ICG-IR−780 = 6.1 vs. free ICG = 2.4 vs. free IR−780 = 2.9; 2.5-fold improvement in FGS contrast Tumor volume at day 14: HSA NP + PTT/PDT = 95 mm^3 vs. free dye + laser = 380 mm^3 vs. untreated = 1200 mm^3 (~92% reduction vs. control) *In vivo* ROS generation (singlet oxygen sensor): 4.2 × higher in HSA-NP group vs. free IR−780 at equivalent molar dose
Song et al. [57]	*FA-IR−780-loaded-NP*	FGS, PTT	*Ovarian cancer*	FGS: 30 mg FA-IR−780-NP/kg i.v. PTT: same dose	FGS: 705 nmPTT: 808 nm, 1 W/cm^2, 10 min	FGS: 48 h PTT: 72 h	Folate receptor-positive cell uptake (OVCAR−3): FA-NPs = 4.8-fold higher intracellular IR−780 vs. non-targeted NPs; confirmed by flow cytometry *In vivo* tumor inhibition rate at day 21: FA-NPs + PTT = 89% vs. non-targeted NPs + PTT = 58% vs. free IR−780 + PTT = 44% vs. untreated = 0% Tumor temperature under 808 nm: FA-NPs = 54.8°C vs. PBS = 37.1°C; complete tumor regression achieved in 3/5 mice after single PTT session
Wang et al. [51]	*Tf-IR−780 NP*	FGS, PTT, PDT	*Colorectal carcinoma (CT26)*	FGS: 0.3 mg IR−780/kg i.v.PTT/PDT: 1 mg/kg i.v.	FGS: 735 nmPTT/PDT: 808 nm, 1 W/cm^2, 5 min	FGS: 48 h PTT/PDT: 24 h	Peak tumor fluorescence at 48 h: Tf-IR−780 NPs = 3.9 × higher signal vs. free IR−780 group at equivalent dose, confirmed by *ex vivo* organ imaging Tumor volume at day 14: Tf-NPs + laser = 110 mm^3 vs. free IR−780 + laser = 490 mm^3 vs. untreated = 1350 mm^3 (~92% inhibition vs. control) Dual PTT/PDT: temperature rise to 52.4°C + ROS (H_2DCFDA assay) 3.6-fold vs. free dye; no significant off-target toxicity in H&E-stained organs
Lu et al. [55]	*HBc-IR−780 VLPs*	FGS, PTT, PDT	*Breast cancer*	FGS: 0.25 mg IR−780/kg i.v.PTT/PDT: 1 mg/kg i.v.	FGS: not specifiedPTT/PDT: 808 nm, 1 W/cm^2, 5 min	FGS: 29 h PTT/PDT: 29 h	Photostability: VLP-IR−780 retained 91% fluorescence intensity after 60 min continuous 808 nm irradiation vs. 48% for free IR−780 Singlet oxygen generation: VLP-IR−780 = 2.8 × higher than free IR−780 at equivalent dye concentration by SOSG assay Tumor inhibition at day 14: HBc VLP + PTT/PDT = 86% vs. free IR−780 + laser = 49% vs. untreated = 0%; complete regression in 2/6 mice

Abbreviations. FGS, fluorescence-guided surgery; PTT, photothermal therapy; PDT, photodynamic therapy; PAI, photoacoustic imaging; SDT, sonodynamic therapy; CT, computed tomography; MRI, magnetic resonance imaging; SERRS, surface-enhanced resonance Raman scattering; i.v., intravenous; ID, injected dose; TBR, tumor-to-background ratio; ROS, reactive oxygen species; SPR, surface plasmon resonance; VLP, virus-like particle; HU, Hounsfield units; N/A, not applicable. Outcome data are expressed relative to the respective control groups reported in each study. Outcome data are derived from the respective referenced studies as reported in the original manuscript. Where exact numerical values were not stated, data are presented as ranges or qualitative comparisons consistent with the source publication.

biocompatibility and clinical translatability; however, they are generally limited by passive targeting mechanisms and potential drug leakage, making them more suitable for short-term imaging or combination therapies rather than precise, long-term drug delivery.

5. Polymeric nanoparticles

Polymeric NPs, particularly those based on biodegradable materials such as poly(lactic-co-glycolic acid) (PLGA), polyethylene glycol (PEG), and related copolymers, have been widely investigated for the delivery of IR−780 [9,41].

PLGA is a biodegradable and biocompatible copolymer approved for several clinical applications, including sustained-release injectable formulations. PEG is commonly used to improve colloidal stability and prolong circulation by reducing nonspecific protein adsorption and delaying clearance. However, PEG is not biologically inert, and repeated exposure may induce anti-PEG antibodies, which can compromise long-term performance. When combined, PLGA and PEG provide complementary formulation advantages: PLGA contributes biodegradability and controlled release, whereas PEG improves dispersion stability and

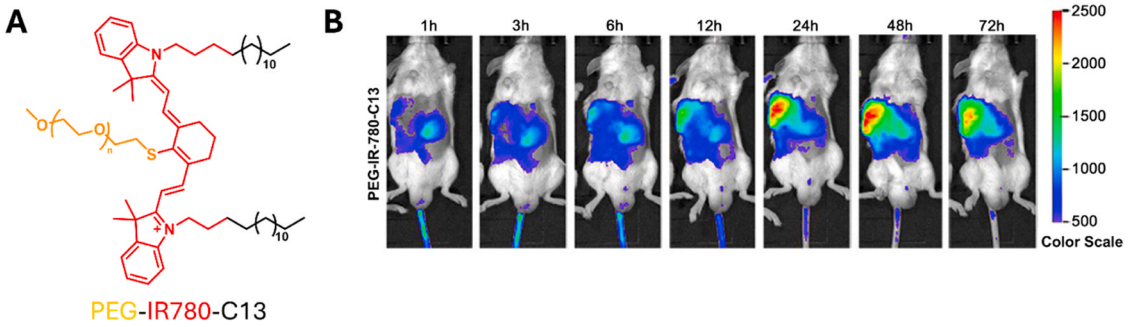


Fig. 4. Yuan *et al.*'s lipid-based NP structure and *in vivo* testing **A)** Chemical structure of the PEG-IR−780-C13**. B)** *In vivo* fluorescence images of PEG-IR−780-C13 micelles at different time points post-injection of PEG-IR−780-C13 micelles (1 mg/kg). Adapted with permission of authors.

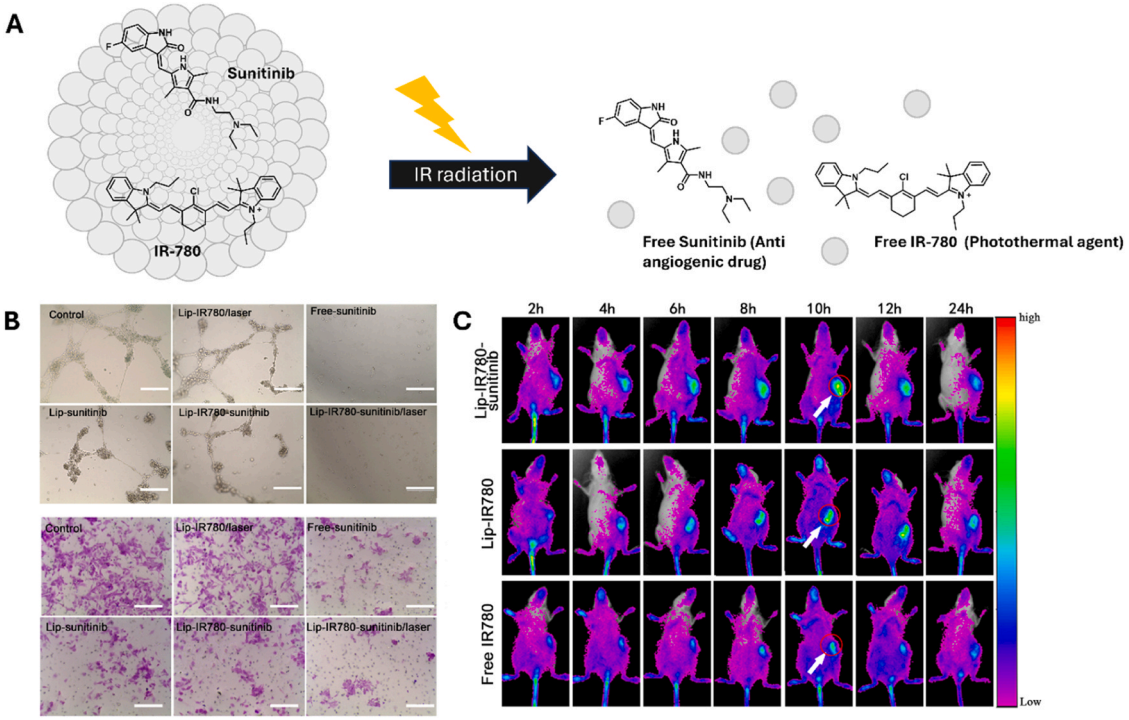


Fig. 5. A) Schematic design of Lip-IR−780-Sunitinib. The drug delivery platform is filled with the antiangiogenic drug sunitinib (hydrophilic) and the photothermal agent IR−780 (lipophilic). When the liposomes are exposed to laser irradiation, the phospholipid membrane ruptures, and Sunitinib is released. **B)** *In vitro* anti-angiogenesis assay with the microscope images show tubule formation by HUVEC on ECMatrix whilst the lower 6 pictures is a result of inhibition of HUVEC cells invasion**. C)** *In vivo* fluorescence images of IR−780 in 4 T1 tumor-bearing mice monitored by *in vivo* imaging after intravenous injection of Lip-IR−780-Sunitinib, LipIR−780 and Free-IR−780.

pharmacokinetic behavior [17].

He and co-authors developed self-assembling polymeric micelles (IPMs) using DSPE-PEG2000 and IR−780 for targeted PTT of breast cancer and its lymphatic metastases (Fig. 6A). These micelles exhibited excellent physicochemical stability in physiological conditions, with high encapsulation efficiency (>95%) and a uniform size (~25.6 nm), favoring tumor penetration and lymphatic accumulation. Following intravenous injection in a metastatic breast cancer model, IPMs preferentially localized in primary tumors and metastatic lymph nodes, as confirmed by *in vivo* and *ex vivo* fluorescence imaging and confocal microscopy (Fig. 6B). Under 808 nm laser irradiation, IPMs generated localized heat (>52 °C), resulting in potent PTT ablation. A single treatment significantly inhibited tumor growth and reduced lymph node metastases by 88.2%, outperforming free IR−780 or non-irradiated controls (Fig. 6C). Moreover, the formulation showed excellent biocompatibility with no significant toxicity [42]. This study demonstrates the potential of IR−780-loaded polymeric micelles as a minimally invasive, effective platform for imaging-guided therapy of primary and metastatic breast cancer.

While He *et al.* demonstrated the potential of IR−780-loaded polymeric micelles for *in vivo* imaging and photothermal ablation of primary tumors and lymphatic metastases, other studies have focused on enhancing the tracking reliability and stability of IR−780 within polymeric nanocarriers [42]. In this context, Machado and co-authors explored two strategies for labeling PLA-PEG nanocapsules with IR−780: physical encapsulation in the oily core versus covalent attachment to the PLA polymer backbone [43]. Using J774A.1 macrophage-like cells, they found that physically encapsulated IR−780 exhibited significant leakage and interaction with serum proteins, leading to high but nonspecific fluorescence signals-raising concerns about whether the observed signal truly reflected nanocarrier uptake or free dye diffusion. In contrast, when IR−780 was covalently attached to PLA by a *copper-free strain-promoted alkyne-azide cycloaddition (SPAAC)* between azide-modified IR−780 and cyclooctyne-functionalized PLA

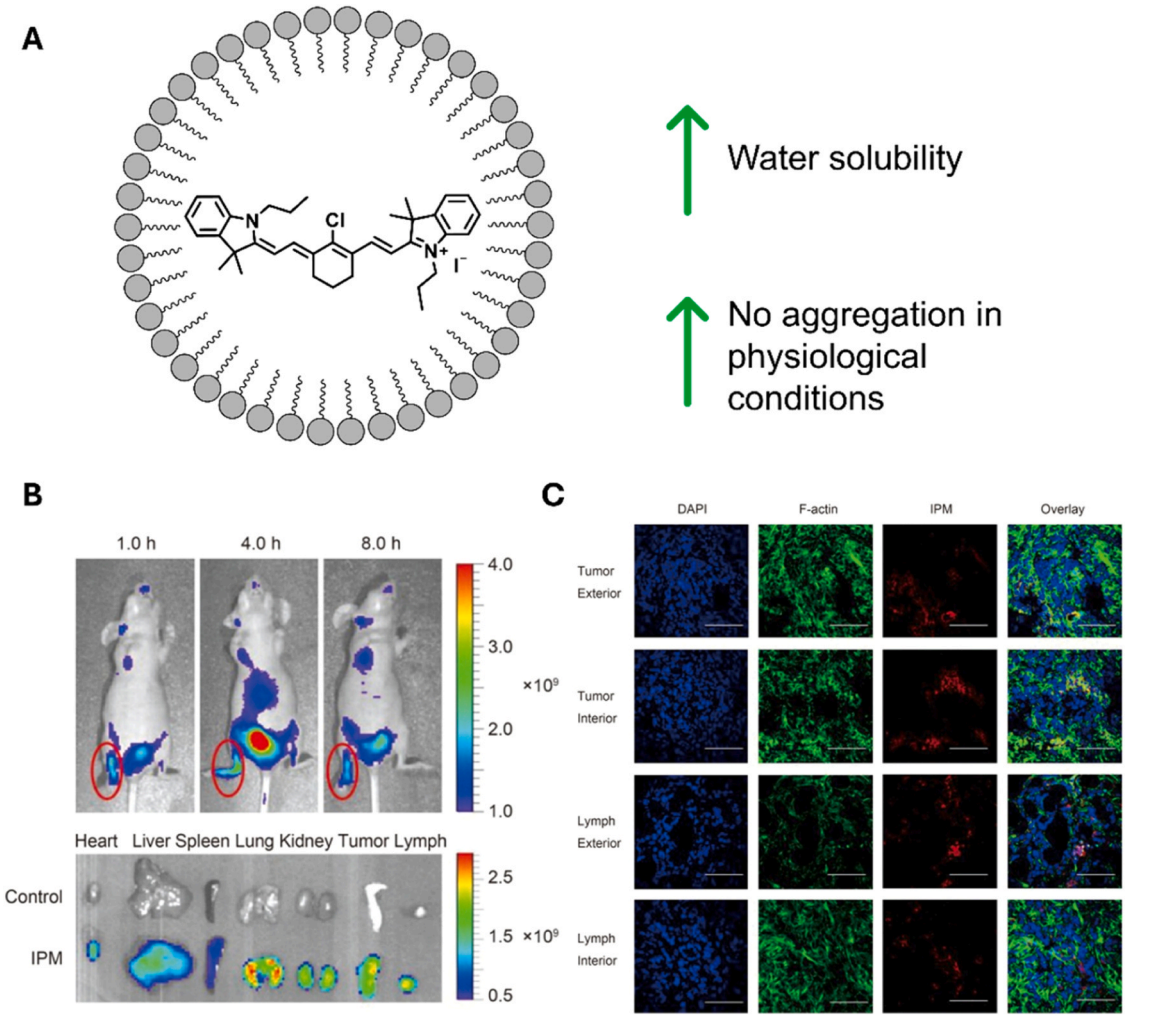


Fig. 6. IR−780-loaded polymeric micelles. **A)** Schematic design of IR−780-loaded micelles **B)** *In vivo* fluorescence imaging of IPMs at 1, 4 and 8 h after injection. **C)** Confocal microscopy showing penetration of IPMs into tumor tissue and metastatic lymph nodes detected after 4 h of injection.

synthesized via ring-opening polymerization, it showed greater stability, reduced premature release, and lower dark toxicity, enabling accurate tracking of nanocarrier internalization. However, this method also required more complex synthesis and showed slightly lower fluorescence intensity due to limited dye loading [43]. Despite these trade-offs, the study highlights covalent conjugation as a more reliable labeling

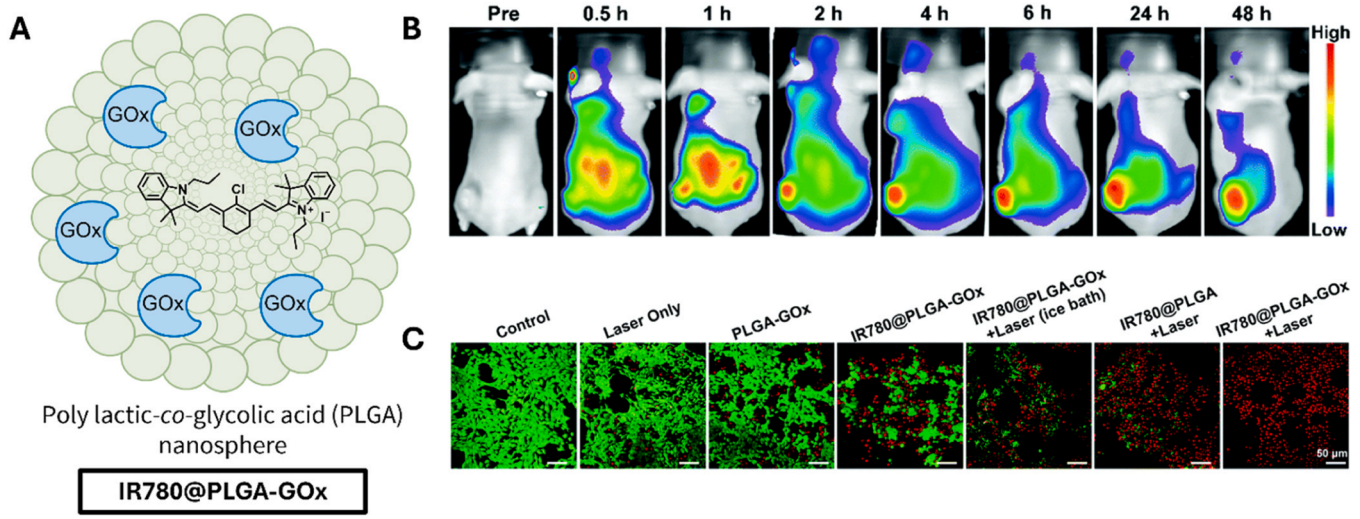


Fig. 7. **A)** Schematic design of the IR−780@PLGA-GOx. **B)** Fluorescence images of 4T1 tumor-bearing mice after intravenous administration of IR−780@PLGA-GOx at various time points **C)** CLSM images of 4T1 cells after various treatments, green representing live cells and the red showing the presence of dead cells.

strategy for preclinical imaging and theranostic applications involving IR−780-loaded polymeric NPs.

In line with the ongoing search for optimized IR−780 delivery systems, Wang *et al.* designed a core–shell PLGA nanosphere (IR−780@PLGA-GOx) combining IR−780 and glucose oxidase (GOx)

to achieve deep tumor penetration, mitochondrial targeting, and synergistic photo/starvation therapy (Fig. 7A). Unlike traditional biomimetic carriers, this platform leveraged IR−780's intrinsic lipophilic cationic properties to enhance both cellular uptake and mitochondrial accumulation, bypassing the need for surface ligands. Notably, the nanospheres showed excellent colloidal stability, high loading efficiency (~80%), and deep distribution in 3D tumor spheroids and *in vivo* models (Fig. 7B). Upon NIR laser irradiation, the system triggered PDT and PTT effects, while GOx-mediated glucose depletion induced starvation, amplifying tumor cell apoptosis (Fig. 7C). The combination of mitochondrial targeting and metabolic disruption led to complete tumor eradication with no recurrence in treated mice [22]. These results underscore the potential of rationally engineered polymeric nanocarriers, distinct from biologically derived membranes, to achieve high targeting precision, deep tissue penetration, and multimodal therapeutic efficacy using IR−780.

Nevertheless, several challenges persist. The encapsulation efficiency of IR−780 may be suboptimal due to its hydrophobic nature, and certain formulations may exhibit an initial burst release, which can compromise treatment control. While photostability is generally enhanced, some degree of photobleaching may still occur under extended laser exposure. Additionally, the fabrication methods can be complex, occasionally necessitating organic solvents or surfactants, thus complicating large-scale production. In some instances, immune clearance may restrict their circulation time.

Compared to lipid-based systems, polymeric NPs provide superior control over drug release and structural stability, but often at the cost of increased formulation complexity and potential issues with reproducibility and scale-up.

6. Inorganic nanoparticles

Inorganic NPs represent another versatile platform for IR−780

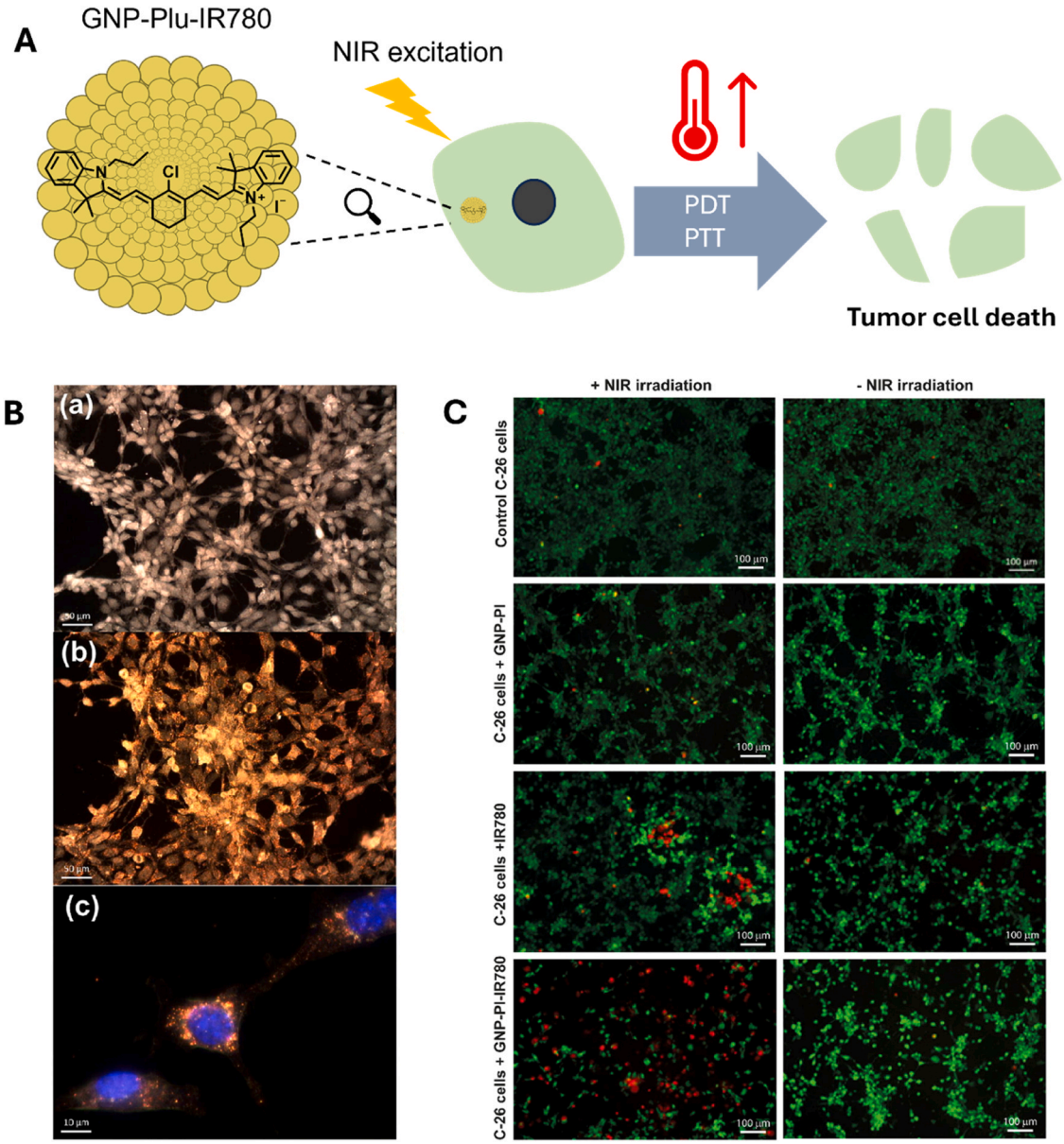


Fig. 8. A) Schematic diagram of GNP-Plu-IR−780 and its mechanism of action. **B)** Dark field image of control C−26 cells incubated with GNP-Plu-IR−780. Merged dark field and fluorescence images (DAPI) of cells incubated with GNP-Plu-IR−780 recorded using a 100x objective. **C)** Merged fluorescence images of C−26 cells.

delivery. Gold NPs (AuNPs), mesoporous silica NPs (MSNs), and iron oxide NPs (Fe_3O_4) are commonly used for their unique optical, magnetic, and structural properties. These materials can serve dual purposes as both carriers and active agents, offering theranostics capabilities. Therapeutic applications of materials such as mesoporous silica, gold nanostructures and upconversion NPs enhance the photostability of IR−780, thereby safeguarding it against degradation and improving its photothermal conversion efficiency [44]. These carriers typically possess high surface areas, facilitating the co-delivery of IR−780 alongside chemotherapeutic agents (e.g., Doxorubicin, Paclitaxel, Cisplatin 5-Fluorouracil), which enables synergistic treatment strategies. Furthermore, their inorganic cores support multimodal imaging techniques (e.g., CT, MRI, photoacoustic), thereby broadening diagnostic capabilities. Surface modifications, including PEGylation or ligand attachment, enhance targeted delivery and enable controlled drug release [9] [45].

Nagi-Simon and co-authors detail the creation of IR−780-loaded gold NPs (GNP-Plu-IR−780), establishing a multifunctional theranostic platform for cancer treatment (Fig. 8A). The gold NPs were synthesized to achieve controlled size and morphology and stabilized with Pluronic F127, which also enabled encapsulation of the hydrophobic dye to integrate the strong surface plasmon resonance and photothermal conversion properties of gold with the dye's tumor-targeting abilities and NIR fluorescence characteristics. Transmission electron microscopy and dynamic light scattering (DLS) analyses confirmed the uniform nanoscale dimensions (~ 48 nm), while UV–Vis–NIR spectroscopy demonstrated both the gold plasmon resonance (~ 522 nm) and IR−780 absorption peaks, signifying successful conjugation. This NP formulation enhanced the aqueous stability of IR−780, diminished photobleaching and ensured sustained colloidal dispersion [46]. Studies on cellular uptake revealed an efficient accumulation of GNP-Plu–IR−780 in tumor cells, attributed to both passive targeting via the EPR effect and the affinity of IR−780 for the mitochondria of cancer cells (Fig. 8B). Upon exposure of GNP-Plu-IR−780-based NPs to NIR laser irradiation, the conjugates produced significant localized heating, resulting in effective photothermal-induced cancer cell death (Fig. 8C). Additionally, NPs enabled high-contrast intracellular imaging through surface-enhanced resonant Raman scattering (SERRS) under NIR excitation.

Nevertheless, inorganic NPs encounter significant challenges. Many of these materials are non-biodegradable and may accumulate in organs, raising concerns regarding toxicity and safety. Their synthesis is often complex, involving multiple steps and the need for precise surface engineering, which can impede reproducibility and scalability. Moreover, despite their promising outcomes in preclinical studies, few have advanced to clinical applications due to regulatory hurdles and a lack of extensive long-term safety data. Additionally, some NPs may exhibit instability in physiological conditions necessitating additional stabilization measures. Overall, while inorganic IR−780 nanocarriers demonstrate considerable therapeutic and diagnostic potential, issues related to toxicity, manufacturing complexities, and clinical translation remain significant obstacles [45].

7. Biomimetic nanoparticles

Biomimetic NPs are engineered to mimic the structure and function of natural biological systems, enhancing their compatibility and performance *in vivo*. This is typically achieved by incorporating cellular components, such as plasma membranes derived from erythrocytes or platelets, which allow the NPs to evade immune clearance and improve targeting. Alternatively, naturally secreted extracellular vesicles, including exosomes, can serve as carriers for therapeutic agents. By leveraging these biologically inspired strategies, biomimetic NPs offer a promising platform for cancer theranostics, combining precise targeting with enhanced biocompatibility [32].

When paired with IR−780, these NPs yield synergistic effects in FGS and phototherapy, while also potentially allowing for the co-delivery of chemotherapeutic agents. The benefits of biomimetic IR−780 NPs include extended circulation time, lower immunogenicity, and enhanced tumor specificity when compared to synthetic alternatives. Their biological surface components promote increased cellular uptake and reduce off-target effects. Moreover, they preserve the photothermal properties of IR−780 and provide controlled release in response to internal stimuli, such as pH or temperature.

This potential is exemplified by the work of Sousa-Junior and co-authors, who developed magnetofluorescent NPs (MMFns) camouflaged with erythrocyte membranes and co-loaded with IR−780 and citrate-coated manganese ferrite ($MnFe_2O_4$) NPs (Fig. 9A). These biomimetic carriers combine magnetic guidance and NIR fluorescence imaging, enabling dual-modal tracking and theranostic applications. In murine models, MMFns showed prolonged circulation (half-life ~92h) and effective tumor accumulation (10% ID at 48 h in Ehrlich tumors), confirmed via 3D fluorescence molecular tomography (FMT) (Fig. 9B). Importantly, stromal modulation using Losartan significantly enhanced delivery efficiency (up to 17.5% ID), emphasizing the role of tumor microenvironment in improving passive targeting [47]. Despite their promise, challenges such as incomplete incorporation of IR−780 and $MnFe_2O_4$, photobleaching, and low magnetic heating efficiency remain. Nevertheless, MMFns illustrate how erythrocyte membrane camouflage can extend circulation time, enhance biodistribution, and support combined imaging and therapeutic functions in IR−780-based nanoplatforms.

Rocha *et al.* further advanced this concept by engineering a multifunctional biomimetic nanoplatform (IR-RM-Mn) incorporating IR−780 into red blood cell (RBC) membrane-coated magnetoliposomes (ML). The biomimetic ML were synthesized in three main steps. First, Mn-doped ferrite NPs were produced via coprecipitation and citrate-coated for colloidal stability. Next, a lipid film of soy phosphatidylcholine (SPC) and cholesterol was hydrated with the NP suspension to form magnetoliposomes, later extruded or sonicated to control size and encapsulation [48]. These synthetic vesicles were then hybridized with cell membranes from RBCs, B16F10 melanoma, or GL261 glioblastoma through repeated freeze–thaw cycles (≈50) at a 4:1 SPC-to-membrane ratio, preserving native membrane proteins. Finally, the near-infrared dye IR−780 was incorporated into the bilayer, yielding multifunctional magnetofluorescent hybrid vesicles with MRI, magnetic hyperthermia, and photothermal therapy capabilities.

This system combined magnetic responsiveness, NIR fluorescence, and PTT within a single construct, achieving tumor ablation with minimal toxicity in a colon cancer mouse model. Compared to Sousa's work, Rocha's platform demonstrated superior photothermal conversion efficiency (25–30%), improved immune evasion, and confirmed *in vivo* effectiveness across multiple administration routes. While both studies underscore the value of RBC membrane camouflage in enhancing biocompatibility and theranostic potential, Rocha and co-authors [48] also highlighted the importance of membrane source selection, magnetic particle clustering, and vesicle formulation on performance, setting the stage for more refined clinical translation of IR−780-based hybrid nanocarriers.

Biomimetic systems exhibit enhanced targeting and immune evasion, yet their biological complexity introduces variability and challenges in standardization, limiting their scalability.

8. Protein-based nanoparticles

Protein-based NPs are constructed from natural or recombinant proteins such as bovine or human serum albumin, gelatin, ferritin and virus-like particles (VLPs). Proteins have been utilized as carriers for IR−780, enabling effective encapsulation or binding through hydrophobic and electrostatic interactions. These NPs preserve the fluorescent and photoabsorbent characteristics of IR−780 while improving its water solubility and circulation time. The benefits of protein-based IR−780

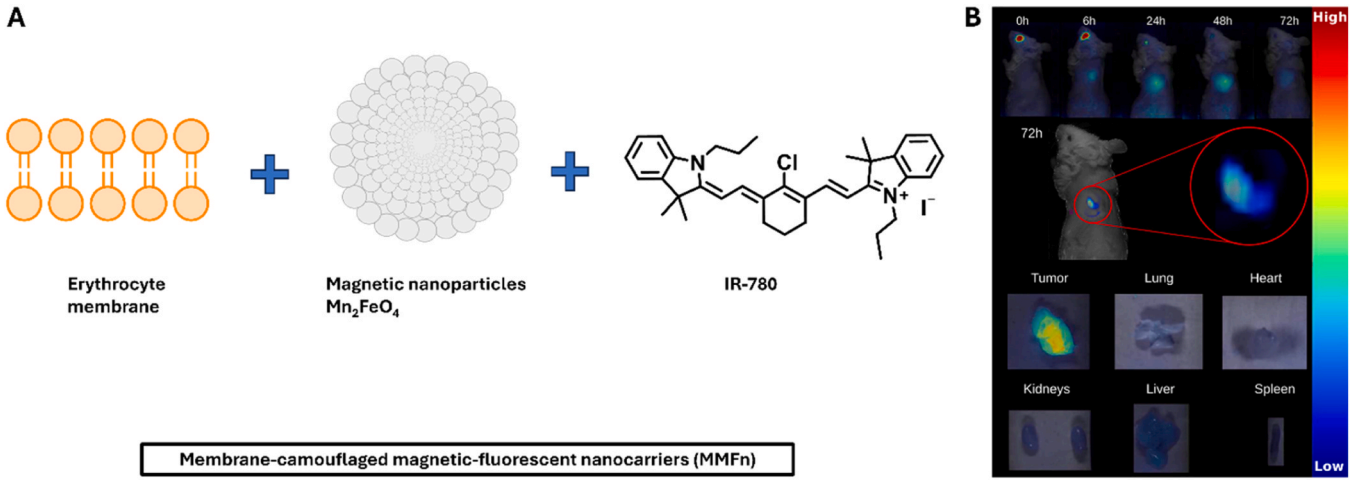


Fig. 9. A) Diagram highlighting components in the MMFn **B)** Series of FMT images and *ex vivo* tests of the mouse at specific time points after retro-orbital administration of MMFns.

NPs include decreased toxicity, enhanced biocompatibility, and the potential for both active and passive targeting. Additionally, the protein matrix offers protection for IR−780 against photodegradation and premature release, thus enhancing therapeutic stability and efficacy [49].

Capistrano and co-authors explored this therapeutic potential by developing albumin-based NPs loaded with IR−780 (AlbIR) for imaging and treatment of Ehrlich tumors in vivo (Fig. 10A/B). Leveraging albumin's natural biocompatibility and tumor-targeting mechanisms via gp60 receptor and SPARC interaction, the formulation showed preferential tumor accumulation and effective PTT ablation following 808 nm laser exposure (Fig. 10C/D). Interestingly, even in the absence of laser irradiation, AlbIR induced significant tumor regression, suggesting an intrinsic chemotherapeutic effect of IR−780 when bound to albumin. The nanocarriers demonstrated improved photostability, prolonged circulation, and tumor-selective cytotoxicity. Histopathological analyses confirmed extensive tumor necrosis and fibrosis with minimal off-target toxicity [50]. While the PTT efficacy was confirmed, the non-photoinduced antitumor mechanism remains incompletely understood, warranting further study. Nevertheless, the combination of imaging, PTT, and spontaneous tumor regression underscores the strong translational potential of albumin-based IR−780 carriers in cancer nanomedicine.

Along similar lines, Wang *et al.* developed a transferrin-based nanoplatform (Tf-IR−780 NP) that expands on the concept of protein-mediated delivery by introducing active targeting via transferrin receptor binding. These NPs were designed for simultaneous PTT and PDT under a single 808 nm laser, and demonstrated remarkable aqueous stability, prolonged circulation ($t_{1/2}$ ~ 20 h), and enhanced tumor uptake through receptor-mediated endocytosis. In a colorectal cancer mouse model, *in vivo* fluorescence imaging confirmed selective tumor accumulation with peak signal at 48 h post-injection (Fig. 11A). Upon NIR laser irradiation (1 W/cm^2, 5 min), Tf-IR−780 NPs induced effective tumor ablation without significant off-target toxicity (Fig. 11B). Notably, *in vitro* and *in vivo* results confirmed dual-functionality: robust ROS generation and local hyperthermia. Transferrin-based NPs offered improved active targeting, though limitations such as moderate liver accumulation and slow dye release (~12% in 48 h) persisted (Fig. 11C) [51]. These findings reinforce the versatility of protein-based IR−780 platforms and highlight transferrin as a promising alternative for receptor-targeted, image-guided phototherapy.

Beyond conventional protein-based carriers such as albumin and transferrin, more structurally sophisticated systems are gaining attention.

For instance, VLPs are self-assembling, protein-based nanocapsules ranging from 20 to 200 nm in size, composed exclusively of viral capsid proteins and lacking any genetic material. As a result, VLPs are inherently non-infectious and offer the advantages of biocompatibility and biodegradability [52]. Their size and morphology can be finely tuned by modifying the terminal amino acids of the capsid proteins, as well as by adjusting buffer pH and thermal conditions during assembly. These NPs closely mimic the structural features of native viruses, enabling enhanced cellular uptake and tumor targeting via both passive and active mechanisms. Their repetitive and symmetrical protein architecture supports stable encapsulation or conjugation of IR−780, preserving its functionality while improving solubility and bioavailability [53,54]. The main advantages of IR−780-loaded VLP include excellent biocompatibility, precise control over particle size, and superior tissue penetration relative to many synthetic carriers. Moreover, their virus-like design promotes efficient cell interaction, making them well-suited for imaging-guided and phototherapy applications. In the realm of virus-like platforms, hepatitis B core (HBc) VLPs have been explored as carriers for IR−780 [55]. The loading of IR−780 was accomplished through a thermal-triggered process conducted at 60°C, leading to the formation of HBc VLP-IR−780 nanostructures. These VLPs exhibited a preferential and sustained accumulation in tumor tissues compared to major organs, which can be attributed to the engineered RGD peptide motif on the external surface of the HBc VLP. The encapsulation of IR−780 within HBc VLP significantly improved its photostability and photothermal conversion efficiency, while also enhancing the generation of ROS compared to the free dye. The HBc VLP-IR−780 system demonstrated strong antitumor efficacy, utilizing the combined advantages of the VLPs' tumor-targeting ability and the dual potential for PTT and PDT offered by IR−780 [55]. However, protein-based carriers may be susceptible to denaturation or aggregation during processing or storage. Furthermore, careful control of protein sources is essential to prevent immunogenicity or contamination [49,56].

Protein-based carriers provide excellent biocompatibility and intrinsic targeting properties, but may suffer from structural instability and limited control over physicochemical properties compared to synthetic systems [49,56].

9. Comparative Evaluation of IR−780 Nanoparticle Platforms

Free IR−780 and NP-based formulations differ substantially in their theranostic performance, pharmacological behavior, and translational potential.

Free IR−780 benefits from chemical simplicity, intrinsic tumor-seeking properties, and easier formulation, but its poor aqueous solubility, rapid clearance, and limited photostability reduce its reproducibility and therapeutic reliability *in vivo* [10,15].

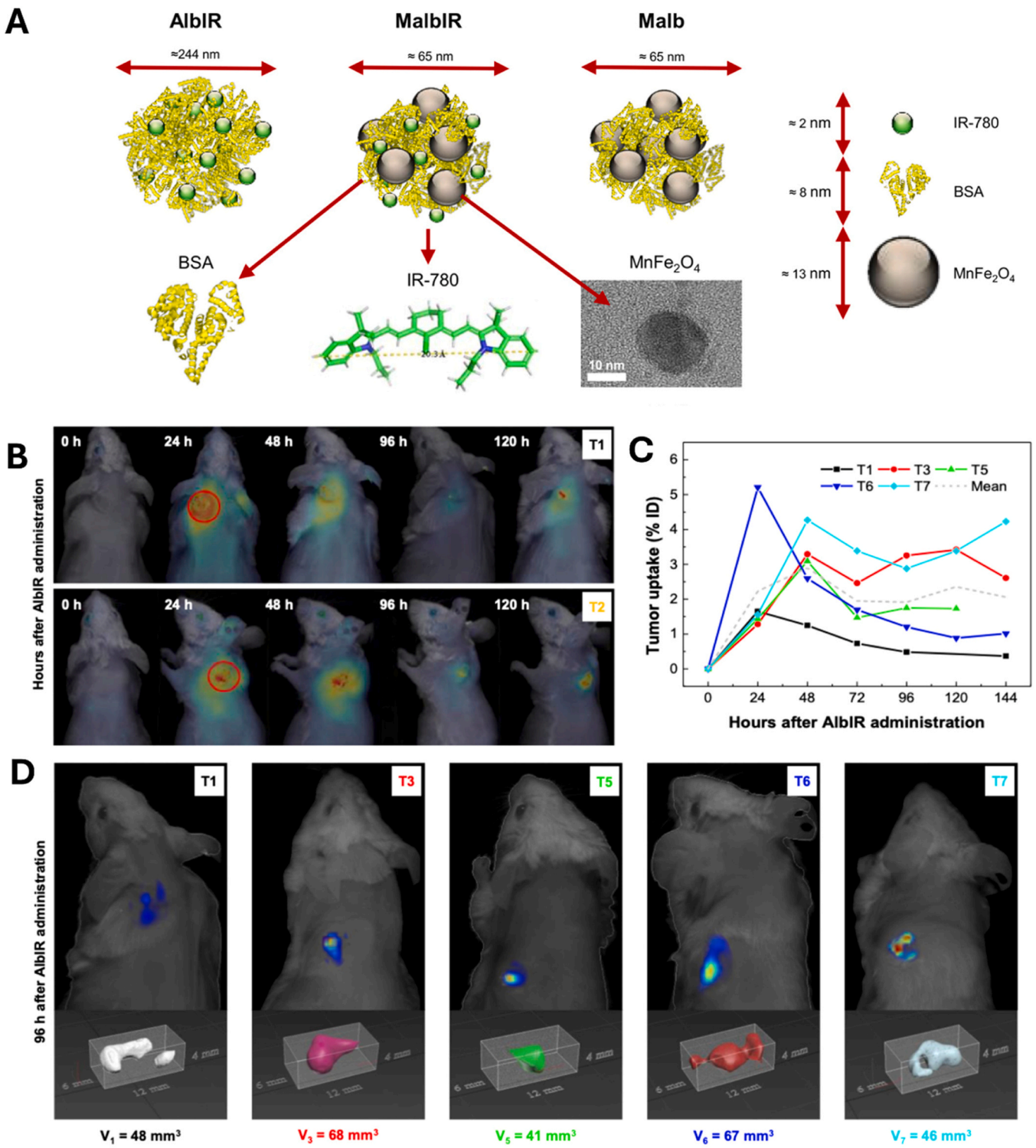


Fig. 10. Albumin-based IR−780 nanoparticles (AlbIR). **A)** Schematic representation of AlbIR nanocarriers **B)** Two-dimensional fluorescence molecular tomography (FMT) images obtained at different time points after AlbIR administration. **C)** Quantification of tumor uptake over time after AlbIR administration. **D)** Representative three-dimensional FMT images obtained 96 h after AlbIR injection for five selected animals.

By contrast, NP-based systems help overcome some of these limitations by improving dye stability, prolonging circulation, increasing tumor retention, and enabling additional functions such as controlled release, active targeting, or multimodal imaging [57]. At the same time, these advantages are not uniform across platforms, and each carrier class introduces its own trade-offs in terms of complexity, safety, scalability, and clinical feasibility [58,59].

Lipid-based NPs are among the most established and clinically familiar systems. Their main strengths are biocompatibility, relative formulation simplicity, and suitability for combination strategies, especially when co-loading therapeutic agents. However, they often rely mainly on passive tumor accumulation through the EPR effect and may be limited by dye leakage or incomplete retention. As a result, they seem more suitable for short-term imaging or triggered combination therapy

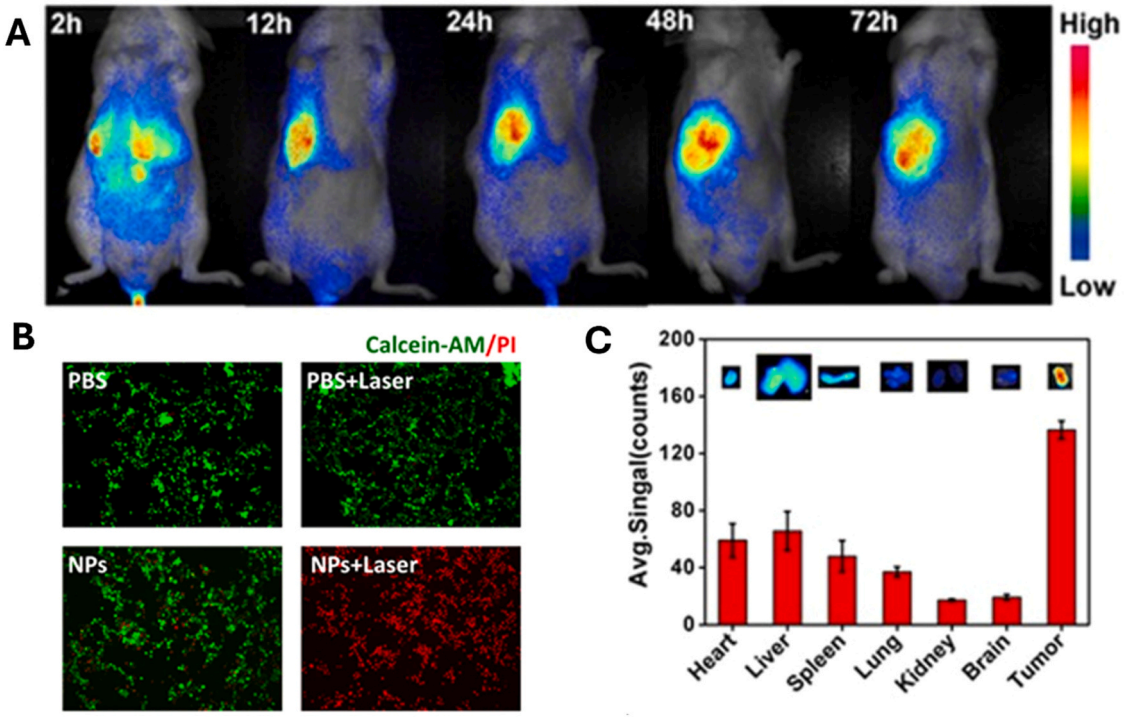


Fig. 11. A) *In vivo* NIR imaging of the mice bearing CT26 tumor injected with Tf-IR−780 NPs (0.3 mg/kg, IR−780) at 2, 12, 24, 48 and 72 h post-injection **B)** Fluorescence images of CT26 cells with the treatments of PBS, PBS plus laser, Tf-IR−780 NPs or Tf-IR−780 NPs plus laser**. C)** E*x vivo* imaging and NIR intensities of Tf-IR−780 NPs in heart, liver, spleen, lung, kidney, brain and tumor of the mice bearing CT26 tumor at 24 h post-injection.

than for highly controlled delivery [15,59].

Polymeric NPs generally provide greater structural stability and better control over payload retention and release. This makes them attractive for sustained therapy, multifunctional platforms, and formulations requiring surface modification or stimulus-responsive behavior. Compared with lipid systems, they are often more versatile, but also more complex to produce, with greater challenges in reproducibility and scale-up [42,60].

Inorganic NPs stand out for their multifunctionality, since the carrier itself often contributes directly to imaging or therapy. Gold, iron oxide, and related systems can enhance photothermal conversion and support modalities such as MRI, CT, photoacoustic imaging or Surface-enhanced Resonance Raman Scattering (SERRS). These features make them appealing for highly integrated theranostic applications, but concerns related to non-biodegradability, long-term accumulation, and manufacturing complexity still limit their translational potential [16,37,61].

Biomimetic NPs offer a different advantage by improving biological performance rather than only physicochemical stability. By incorporating erythrocyte membranes, cancer-cell membranes, or extracellular vesicle-like components, these systems can prolong circulation, reduce immune clearance, and in some cases enhance tumor homing. However, this biological sophistication comes with greater variability, more difficult standardization, and major scale-up challenges [32,47].

Protein-based NPs occupy an intermediate position between synthetic simplicity and biological functionality. Albumin-, transferrin-, and virus-like particle-based systems can improve solubility, photostability, and tumor interaction while taking advantage of endogenous uptake pathways or receptor-mediated targeting. In this sense, they may represent a more realistic translational compromise than some biomimetic or inorganic systems, although issues such as denaturation, source variability, and immunogenicity still need to be considered [9,13].

Overall, no single IR−780 formulation is universally superior. Rather, each platform addresses a different limitation of the free dye. Free IR−780 or simple lipid systems may be sufficient when rapid tumor localization and formulation simplicity are the main priorities, whereas polymeric, biomimetic, or protein-based carriers may be more appropriate when longer circulation, tighter delivery control, or improved biological targeting are required. Inorganic systems remain especially attractive for multimodal imaging and strong PTT performance, despite their safety and translational limitations [9,10]. The field is therefore moving toward a more application-specific approach, in which the most suitable formulation depends on the particular therapeutic or pharmacological challenge that needs to be addressed.

10. Clinical perspective and translational challenges

While extensive preclinical studies have demonstrated the theranostic potential of IR−780-based systems, clinical translation remains limited. To date, no IR−780-based nanomedicine has received regulatory approval, and clinical evaluation of IR−780-derived theranostics systems remains very limited [10].

In contrast, other NIR dyes such as ICG, IRDye800CW and IRDye700DX, have advanced into clinical use or clinical trials, particularly in FGS, supported by well-established safety profiles and standardized manufacturing processes [62−65].

This highlights the current lack of regulatory familiarity and standardization for IR−780-based platforms [66,67].

Several factors contribute to this gap. First, the absence of standardized evaluation protocols limits reproducibility, as studies vary widely in tumor models, dosing regimens, and treatment parameters. Second, large-scale manufacturing remains challenging, especially for complex NP systems, affecting batch consistency, cost, and scalability. Third, IR−780 exhibits rapid clearance and short systemic half-life, while NP formulations, although extending circulation time, raise concerns about long-term biodistribution and safety. Inorganic systems further face issues related to non-biodegradability and potential accumulation [50,51,68].

Additionally, regulatory approval requires comprehensive

characterization of toxicity, immune interactions, and degradation pathways, which is complicated by the structural complexity of multifunctional nanoplatforms. Although IR−780 shows intrinsic tumor selectivity, this is not universal, and the incorporation of active targeting ligands, while improving specificity, adds further complexity and potential immunogenicity [18,51,69].

Overall, successful clinical translation will require standardized protocols, scalable and reproducible manufacturing, and stronger alignment with regulatory requirements, alongside further biological and clinical validation.

11. Strengths and Limitations

IR−780 is an appealing theranostic scaffold because it combines intrinsic tumor affinity with imaging and therapeutic functionality in a single small molecule. Unlike many targeted fluorophores, it does not necessarily require conjugation to antibodies or ligands to achieve tumor accumulation, as its uptake appears to be driven, at least in part, by mitochondrial membrane potential and OATP-related transport in malignant cells [9−11].

In addition to NIR fluorescence imaging, IR−780 also supports PDT and PTT effects, which broadens its relevance from tumor visualization to light-activated treatment strategies [13−15].

Its structural versatility has further encouraged the development of analogues and derivatives designed to improve optical output, pharmacological behavior, and overall theranostic performance [20,23,26].

The principal weakness of free IR−780 lies in its limited pharmaceutical suitability rather than in its biological potential. Poor water solubility, susceptibility to photodegradation, and rapid clearance restrict its reproducibility and narrow its therapeutic window *in vivo* [16,22].

Nanocarrier-based delivery has therefore emerged less as an optional refinement and more as a necessary strategy to unlock the dye's practical utility. Across the literature, lipid, polymeric, inorganic, biomimetic, and protein-based systems have each demonstrated the capacity to improve selected aspects of IR−780 performance, including colloidal stability, tumor retention, biodistribution, and therapeutic precision, while also enabling combination therapies and multimodal imaging designs [10,17,33,38,44].

Yet, the breadth of formulation strategies has not translated into conceptual clarity. One of the major limitations of the current field is the lack of standardization in experimental design and reporting. Differences in NP composition, tumor model, dose, administration route, irradiation settings, and endpoint selection make it difficult to determine whether apparent performance differences reflect genuine platform superiority or simply divergent study conditions [10]. Moreover, the limitations are not uniform across carriers: lipid systems may be limited by premature leakage, polymeric systems by formulation complexity, inorganic systems by persistence and uncertain long-term safety, biomimetic systems by poor standardizability, and protein-based carriers by structural fragility or immunogenicity [37,42] [45,47,56].

A further concern is that most available studies remain confined to simplified preclinical settings. The heavy reliance on subcutaneous murine xenografts likely overestimates EPR-dependent accumulation and does not adequately capture the biological barriers encountered in human tumors. Orthotopic, patient-derived, and large-animal models remain comparatively underrepresented, despite being more informative for translational assessment [70,71].

In parallel, issues such as scalable manufacturing, GMP compatibility, long-term biodistribution, and robust toxicological characterization are still insufficiently addressed.

Taken together, the available evidence suggests that no single IR−780 platform is universally optimal. Lipid-based and protein-based systems appear the most attractive for relatively simple and biocompatible formulations, particularly for imaging or combination approaches. Polymeric systems offer greater control over payload retention and release and are therefore more suitable for engineered multifunctional therapy. Inorganic systems remain particularly attractive when strong photothermal conversion or multimodal imaging is required, although their translational profile is weaker because of safety and persistence concerns. Biomimetic platforms may offer superior biological behavior, but their complexity and limited standardization remain major obstacles to scale-up.

12. Conclusions

Overall, IR−780 remains a highly attractive theranostic scaffold because it combines intrinsic tumor affinity with fluorescence imaging and light-activated therapeutic potential. However, the free dye is constrained by poor aqueous solubility, limited formulation robustness, and suboptimal in vivo reproducibility. Nanoencapsulation can address many of these limitations, but the translational value of each platform depends on the balance between functional sophistication and manufacturability. Future progress in the field will require more standardized comparative studies, clinically relevant tumor models, robust pharmacokinetic and toxicological evaluation, and formulation strategies that are compatible with scalable manufacturing and regulatory development.

CRediT authorship contribution statement

Giulia Lanfranchi: Writing – original draft. **Laura Privitera:** Writing – review & editing. **Adam Sedgwick:** Writing – review & editing, Resources. **Gloria Pelizzo:** Validation, Supervision. **Michela Marinaro:** Writing – original draft, Investigation. **Raouf El-Dabl:** Resources, Methodology. **Irene Paraboschi:** Writing – original draft, Investigation, Conceptualization. **Stefano Giuliani:** Writing – review & editing, Validation, Supervision.

Declaration of Competing Interest

The authors declare that there are no conflicts of interest regarding the publication of this article. The authors alone are responsible for the content and the writing of the manuscript.

References

[1] B.J. Burkett, D.J. Bartlett, P.W. McGarrah, A.R. Lewis, D.R. Johnson, K. Berberoğlu, et al., A review of theranostics: perspectives on emerging approaches and clinical advancements, Radiol. Imaging Cancer 5 (4) (2023 Jul 1), https://doi.org/10.1148/rycan.220157.

[2] T. Ahmed, M.V. Pai, E. Mallik, G.M. Varghese, S. Ashish, A. Acharya, et al., Applications of indocyanine green in surgery: A single center case series, Ann. Med. Surg. (2022 May 1) 77, https://doi.org/10.1016/j.amsu.2022.103602.

[3] Y. Gao, L. Zhu, Z. Du, J. Xiong, R. Ma, M. Aili, et al., Recent advances in near-infrared cyanine dye-based fluorescent nanoprobes for tumor imaging and therapy, Int. J. Nanomed. 20 (2025) 13911–13937, https://doi.org/10.2147/IJN.S542880.

[4] S. Giuliani, I. Paraboschi, A. McNair, M. Smith, K.S. Rankin, D.S. Elson, et al., Monoclonal antibodies for targeted fluorescence-guided surgery: a review of applicability across multiple solid tumors, Cancers 16 (5) (2024 Mar 4) 1045, https://doi.org/10.3390/cancers16051045.

[5] D.M. Polikarpov, D.H. Campbell, L.S. McRobb, J. Wu, M.E. Lund, Y. Lu, et al., Near-infrared molecular imaging of glioblastoma by Miltuximab®-IRDye800CW as a potential tool for fluorescence-guided surgery, Cancers 12 (4) (2020 Apr 16) 984, https://doi.org/10.3390/cancers12040984.

[6] L. Privitera, D.J. Waterhouse, A. Preziosi, I. Paraboschi, O. Ogunlade, C. Da Pieve, et al., Shortwave infrared imaging enables high-contrast fluorescence-guided surgery in neuroblastoma, Cancer Res. 83 (12) (2023 Jun 15) 2077–2089, https://doi.org/10.1158/0008-5472.CAN-22-2918.

[7] B. Zohuri, H. Zand, Near-Infrared vs. Mid-Infrared Light Penetration in Biological Tissues, Med. Clin. Res. 10 (03) (2025 Mar 20) 01–09, https://doi.org/10.33140/MCR.10.03.04.

[8] C. Zhang, T. Liu, Y. Su, S. Luo, Y. Zhu, X. Tan, et al., A near-infrared fluorescent heptamethine indocyanine dye with preferential tumor accumulation for in vivo imaging, Biomaterials 31 (25) (2010 Sep) 6612–6617, https://doi.org/10.1016/j.biomaterials.2010.05.007.

[9] M.C.P. Fialho, M.A. de Oliveira, M.G.C. Machado, C.M. Lacerda, V.C.F. Mosqueira, IR-780-based nanotheranostics and in vivo effects: a review, J. Nanotheranostics 6 (1) (2025 Mar 7) 8, https://doi.org/10.3390/jnt6010008.

[10] C.G. Alves, R. Lima-Sousa, D. de Melo-Diogo, R.O. Louro, I.J. Correia, IR-780 based nanomaterials for cancer imaging and photothermal, photodynamic and combinatorial therapies. International Journal of Pharmaceutics, Elsevier B.V, 2018, pp. 164–175, https://doi.org/10.1016/j.ijpharm.2018.03.020.

[11] M.C. Tsai, L.Y. Hsiao, Y.H. Chang, Y.H. Chen, S.H. Hu, C.Y. Hung, et al., Enhanced intracellular IR-780 delivery by acidity-triggered PEG-detachable hybrid nanoparticles to augment photodynamic and photothermal combination therapy for melanoma treatment, ACS Appl. Bio Mater. 8 (5) (2025 May 19) 3995–4007, https://doi.org/10.1021/acsabm.5c00144.

[12] M.G.C. Machado, M.A. de Oliveira, E.G. Lanna, R.P. Siqueira, G. Pound-Lana, R. T. Branquinho, et al., Photodynamic therapy with the dual-mode association of IR-780 to PEG-PLA nanocapsules and the effects on human breast cancer cells, Biomed. & Pharmacother. 145 (2022 Jan) 112464, https://doi.org/10.1016/j.biopha.2021.112464.

[13] J. Yang, W. Wang, S. Huang, D. Guo, L. Yu, W. Qiao, et al., Production, Characterization, and Application of Hydrophobin-Based IR-780 Nanoparticles for Targeted Photothermal Cancer Therapy and Advanced Near-Infrared Imaging. Adv Healthc, Mater 14 (1) (2025 Jan 3), https://doi.org/10.1002/adhm.202402311.

[14] H. Rezaei Far, M. Amiri, Z. Elyasigorji, E. Heydari, M. Saviz, Faraji-Dana R, et al. Photothermal Oxygen-Releasing IR-780/CaO $_2$ Nanoplatform for Enhanced and On-Demand Photodynamic Therapy, ACS Appl. Nano Mater. 7 (20) (2024 Oct 25) 23627–23640, https://doi.org/10.1021/acsanm.4c03929.

[15] Y.J. Lu, A.T. S, C.C. Chuang, J.P. Chen, Liposomal IR-780 as a Highly Stable Nanotheranostic Agent for Improved Photothermal/Photodynamic Therapy of Brain Tumors by Convection-Enhanced Delivery, Cancers (Basel) 13 (15) (2021 Jul 22) 3690, https://doi.org/10.3390/cancers13153690.

[16] Z. Mo, M. Qiu, K. Zhao, H. Hu, Q. Xu, J. Cao, et al., Multifunctional phototheranostic nanoplatform based on polydopamine-manganese dioxide-IR-780 iodide for effective magnetic resonance imaging-guided synergistic photodynamic/photothermal therapy, J. Colloid Interface Sci. 611 (2022 Apr) 193–204, https://doi.org/10.1016/j.jcis.2021.12.071.

[17] D. Zhang, L. Liu, J. Wang, H. Zhang, Z. Zhang, G. Xing, et al., Drug-loaded PEG-PLGA nanoparticles for cancer treatment, Front. Pharmacol. Front. Media S. A (2022), https://doi.org/10.3389/fphar.2022.990505.

[18] M.J. Mitchell, M.M. Billingsley, R.M. Haley, M.E. Wechsler, N.A. Peppas, R. Langer, Engineering precision nanoparticles for drug delivery, Nat. Rev. Drug. Discov. 20 (2) (2021 Feb 4) 101–124, https://doi.org/10.1038/s41573-020-0090-8.

[19] C. Canovas, P.S. Bellaye, M. Moreau, A. Romieu, F. Denat, V. Goncalves, Site-specific near-infrared fluorescent labelling of proteins on cysteine residues with *meso* -chloro-substituted heptamethine cyanine dyes, Org. Biomol. Chem. 16 (45) (2018) 8831–8836, https://doi.org/10.1039/C8OB02646G.

[20] X. Zhao, F. Zhang, Z. Lei, The pursuit of polymethine fluorophores with NIR-II emission and high brightness for, vivo Appl. Chem. Sci. 13 (38) (2022) 11280–11293, https://doi.org/10.1039/D2SC03136A.

[21] E. Zhang, S. Luo, X. Tan, C. Shi, Mechanistic study of IR-780 dye as a potential tumor targeting and drug delivery agent, Biomaterials 35 (2) (2014 Jan) 771–778, https://doi.org/10.1016/j.biomaterials.2013.10.033.

[22] Y. Wang, B. Wang, L. Zhang, J. Huang, P. Li, Y. Zhao, et al., Mitochondria-targeted nanospheres with deep tumor penetration for photo/starvation therapy, J. Mater. Chem. B 8 (34) (2020) 7740–7754, https://doi.org/10.1039/D0TB00001A.

[23] S.M. Usama, C.M. Lin, K. Burgess, On the Mechanisms of Uptake of Tumor-Seeking Cyanine Dyes, Bioconjug Chem. 29 (11) (2018 Nov 21) 3886–3895, https://doi.org/10.1021/acs.bioconjchem.8b00708.

[24] R. Margolis, L. Basavarajappa, J. Li, G. Obaid, K. Hoyt, Image-guided focused ultrasound-mediated molecular delivery to breast cancer in an animal model, Phys. Med. Biol. 68 (15) (2023 Jul 21), https://doi.org/10.1088/1361-6560/ace23d.

[25] Z. He, L. Zhang, L. Xing, W. Sun, X. Gao, Y. Zhang, et al., IR-780-based diffuse fluorescence tomography for cancer detection, J. Biophotonics 17 (5) (2024 May 8), https://doi.org/10.1002/jbio.202300493.

[26] S. Zhu, B.C. Yung, S. Chandra, G. Niu, A.L. Antaris, X. Chen, Near-Infrared-II (NIR-II) Bioimaging *via* Off-Peak NIR-I Fluorescence Emission, Theranostics 8 (15) (2018) 4141–4151, https://doi.org/10.7150/thno.27995.

[27] S.M. Usama, G.K. Park, S. Nomura, Y. Baek, H.S. Choi, K. Burgess, Role of Albumin in Accumulation and Persistence of Tumor-Seeking Cyanine Dyes, Bioconjug Chem. 31 (2) (2020 Feb 19) 248–259, https://doi.org/10.1021/acs.bioconjchem.9b00771.

[28] C. Zhang, L. Long, C. Shi, Mitochondria-targeting IR-780 dye and its derivatives: synthesis, mechanisms of action, and theranostic applications, Adv. Ther. (Weinh.) (7) (2018 Nov 9) 1, https://doi.org/10.1002/adtp.201800069.

[29] S.M. Usama, S. Thavornpradit, K. Burgess, Optimized Heptamethine Cyanines for Photodynamic Therapy, ACS Appl. Bio Mater. 1 (4) (2018 Oct 15) 1195–1205, https://doi.org/10.1021/acsabm.8b00414.

[30] Y. Wang, T. Liu, E. Zhang, S. Luo, X. Tan, C. Shi, Preferential accumulation of the near infrared heptamethine dye IR-780 in the mitochondria of drug-resistant lung cancer cells, Biomaterials 35 (13) (2014 Apr) 4116–4124, https://doi.org/10.1016/j.biomaterials.2014.01.061.

[31] B.E. Mc Larney, A.Y. Sonay, E. Apfelbaum, N. Mostafa, S. Monette, D. Goerzen, et al., A pan-cancer dye for solid-tumor screening, resection and wound monitoring via short-wave and near-infrared fluorescence imaging, Nat. Biomed. Eng. 8 (9) (2024 Sep 9) 1092–1108, https://doi.org/10.1038/s41551-024-01248-w.

[32] L. Wang, C. Niu, IR-780-based nanomaterials for cancer imaging and therapy. Journal of Materials Chemistry B, Royal Society of Chemistry, 2021, pp. 4079–4097, https://doi.org/10.1039/d1tb00407g.

[33] A. Auger, J. Samuel, O. Poncelet, O. Raccurt, A comparative study of non-covalent encapsulation methods for organic dyes into silica nanoparticles, Nanoscale Res. Lett. 6 (1) (2011 Apr 13) 328, https://doi.org/10.1186/1556-276X-6-328.

[34] H. Chen, Q. Hu, W. Li, X. Cai, L. Mao, R. Li, Approaches to Nanoparticle Labeling: A Review of Fluorescent, Radiological, and Metallic Techniques, Environ. & Health 1 (2) (2023 Aug 18) 75–89, https://doi.org/10.1021/envhealth.3c00034.

[35] O.S. Wolfbeis, An overview of nanoparticles commonly used in fluorescent bioimaging, Chem. Soc. Rev. 44 (14) (2015) 4743–4768, https://doi.org/10.1039/C4CS00392F.

[36] G. Vargas-Nadal, M. Köber, A. Nsamela, F. Terenziani, C. Sissa, S. Pescina, et al., Fluorescent Multifunctional Organic Nanoparticles for Drug Delivery and Bioimaging: A Tutorial Review, Pharmaceutics 14 (11) (2022 Nov 17) 2498, https://doi.org/10.3390/pharmaceutics14112498.

[37] J.M. Barcelos, T.G. Hayasaki, R.C. de Santana, E.M. Lima, S.A. Mendanha, A. F. Bakuzis, Photothermal Properties of IR-780-Based Nanoparticles Depend on Nanocarrier Design: A Comparative Study on Synthetic Liposomes and Cell Membrane and Hybrid Biomimetic Vesicles, Pharmaceutics 15 (2) (2023 Feb 1), https://doi.org/10.3390/pharmaceutics15020444.

[38] A. Yuan, X. Qiu, X. Tang, W. Liu, J. Wu, Y. Hu, Self-assembled PEG-IR-780-C13 micelle as a targeting, safe and highly-effective photothermal agent for in vivo imaging and cancer therapy, Biomaterials 51 (2015 May) 184–193, https://doi.org/10.1016/j.biomaterials.2015.01.069.

[39] X. Yang, H. Li, C. Qian, Y. Guo, C. Li, F. Gao, et al., Near-infrared light-activated IR-780-loaded liposomes for anti-tumor angiogenesis and Photothermal therapy, Nanomedicine 14 (7) (2018 Oct 1) 2283–2294, https://doi.org/10.1016/j.nano.2018.06.011.

[40] I. Waheed, A. Ali, H. Tabassum, N. Khatoon, W.F. Lai, X. Zhou, Lipid-based nanoparticles as drug delivery carriers for cancer therapy, Front. Oncol. 14 (2024) 1296091, https://doi.org/10.3389/fonc.2024.1296091.

[41] Y. Gao, K. Wang, J. Zhang, X. Duan, Q. Sun, K. Men, Multifunctional nanoparticle for cancer therapy, MedComm (Beijing) 4 (1) (2023 Feb) e187, https://doi.org/10.1002/mco2.187.

[42] B. He, H. yan Hu, T. Tan, H. Wang, K. xiang Sun, Y. ping Li, et al., IR-780-loaded polymeric micelles enhance the efficacy of photothermal therapy in treating breast cancer lymphatic metastasis in mice, Acta Pharmacol. Sin. 39 (1) (2018 Jan 10) 132–139, https://doi.org/10.1038/aps.2017.109.

[43] M.G.C. Machado, G. Pound-Lana, M.A. de Oliveira, E.G. Lanna, M.C.P. Fialho, A.C. F. de Brito, et al., Labeling PLA-PEG nanocarriers with IR-780: physical entrapment versus covalent attachment to polylactide, Drug. Deliv. Transl. Res. 10 (6) (2020 Dec) 1626–1643, https://doi.org/10.1007/s13346-020-00812-6.

[44] M. Gu, W. Yu, H. Wu, C. Fu, R. Du, IR-780-Loaded Polydopamine Nanoparticles for Synergistic Photodynamic and Photothermal Therapy, ACS Appl. Nano Mater. 8 (42) (2025 Oct 24) 20329–20340, https://doi.org/10.1021/acsanm.5c03531.

[45] W. Li, Z. Cao, R. Liu, L. Liu, H. Li, X. Li, et al., AuNPs as an important inorganic nanoparticle applied in drug carrier systems, Artif. Cells Nanomed. Biotechnol. 47 (1) (2019 Dec 4) 4222–4233, https://doi.org/10.1080/21691401.2019.1687501.

[46] T. Nagy-Simon, M. Potara, A.M. Craciun, E. Licarete, S. Astilean, IR-780-dye loaded gold nanoparticles as new near infrared activatable nanotheranostic agents for simultaneous photodynamic and photothermal therapy and intracellular tracking by surface enhanced resonant Raman scattering imaging, J. Colloid Interface Sci. 517 (2018 May) 239–250, https://doi.org/10.1016/j.jcis.2018.02.007.

[47] A.A. Sousa-Junior, S.A. Mendanha, M.S. Carrião, G. Capistrano, A.G. Próspero, G. A. Soares, et al., Predictive Model for Delivery Efficiency: Erythrocyte Membrane-Camouflaged Magnetofluorescent Nanocarriers Study, Mol. Pharm. 17 (3) (2020 Mar 2) 837–851, https://doi.org/10.1021/acs.molpharmaceut.9b01094.

[48] J.V.R. Rocha, R.F. Krause, C.E. Ribeiro, N.C. Oliveira, A. de, L. Ribeiro de Sousa, J. Leandro Santos, et al., Near Infrared Biomimetic Hybrid Magnetic Nanocarrier for MRI-Guided Thermal Therapy, ACS Appl. Mater. Interfaces 17 (9) (2025 Mar 5) 13094–13110, https://doi.org/10.1021/acsami.4c03434.

[49] X. Guo, J. Mei, C. Zhang, Development of Drug Dual-Carriers Delivery System with Mitochondria-Targeted and pH/Heat Responsive Capacity for Synergistic Photothermal-Chemotherapy of Ovarian Cancer, Int. J. Nanomed. 15 (2020 Jan) 301–313, https://doi.org/10.2147/IJN.S226517.

[50] G. Capistrano, A.A. Sousa-Junior, R.A. Silva, F. Mello-Andrade, E.R. Cintra, S. Santos, et al., IR-780-Albumin-Based Nanocarriers Promote Tumor Regression Not only from Phototherapy but Also by a Nonirradiation Mechanism, ACS Biomater. Sci. Eng. 6 (8) (2020 Aug 10) 4523–4538, https://doi.org/10.1021/acsbiomaterials.0c00164.

[51] K. Wang, Y. Zhang, J. Wang, A. Yuan, M. Sun, J. Wu, et al., Self-assembled IR-780-loaded transferrin nanoparticles as an imaging, targeting and PDT/PTT agent for cancer therapy, Sci. Rep. 6 (1) (2016 Jun 6) 27421, https://doi.org/10.1038/srep27421.

[52] M. Comas-Garcia, M. Colunga-Saucedo, S. Rosales-Mendoza, The Role of Virus-Like Particles in Medical Biotechnology, Mol. Pharm. 17 (12) (2020 Dec 7) 4407–4420, https://doi.org/10.1021/acs.molpharmaceut.0c00828.

[53] K.R. Kim, A.S. Lee, S.M. Kim, H.R. Heo, C.S. Kim, Virus-like nanoparticles as a theranostic platform for cancer, Front. Bioeng. Biotechnol. (2023 Jan 12) 10, https://doi.org/10.3389/fbioe.2022.1106767.

[54] G. Wang, T. Jia, X. Xu, L. Chang, R. Zhang, Y. Fu, et al., Novel miR-122 delivery system based on MS2 virus like particle surface displaying cell-penetrating peptide TAT for hepatocellular carcinoma, Oncotarget 7 (37) (2016 Sep 13) 59402–59416, https://doi.org/10.18632/oncotarget.10681.

[55] F. Lu, Z. Li, Y. Sheng, Y. Ma, Y. Yang, Y. Ren, et al., Thermal-triggered packing of lipophilic NIR dye IR-780 in hepatitis B core at critical ionic strength and cargo-host ratio for improved stability and enhanced cancer phototherapy, Biomaterials (2021 Sep 1) 276, https://doi.org/10.1016/j.biomaterials.2021.121035.

[56] M.A. de Oliveira, G. Pound-Lana, P. Capelari-Oliveira, T.G. Pontífice, S.E.D. Silva, M.G.C. Machado, et al., Release, transfer and partition of fluorescent dyes from polymeric nanocarriers to serum proteins monitored by asymmetric flow field-flow fractionation, J. Chromatogr. A 1641 (2021 Mar) 461959, https://doi.org/10.1016/j.chroma.2021.461959.
[57] J. Song, N. Zhang, L. Zhang, H. Yi, Y. Liu, Y. Li, et al., IR-780-loaded folate-targeted nanoparticles for near-infrared fluorescence image-guided surgery and photothermal therapy in ovarian cancer, Int. J. Nanomed. 14 (2019) 2757–2772, https://doi.org/10.2147/IJN.S203108.
[58] N. Desai, Challenges in development of nanoparticle-based therapeutics, AAPS J. 14 (2) (2012 Jun) 282–295, https://doi.org/10.1208/s12248-012-9339-4.
[59] S. Gavas, S. Quazi, T.M. Karpiński, Nanoparticles for Cancer Therapy: Current Progress and Challenges, Nanoscale Res. Lett. 16 (1) (2021 Dec 5) 173, https://doi.org/10.1186/s11671-021-03628-6.
[60] R.X. Zhang, T. Ahmed, L.Y. Li, J. Li, A.Z. Abbasi, X.Y. Wu, Design of nanocarriers for nanoscale drug delivery to enhance cancer treatment using hybrid polymer and lipid building blocks, Nanoscale 9 (4) (2017) 1334–1355, https://doi.org/10.1039/C6NR08486A.
[61] S.Y. Lin, R.Y. Huang, W.C. Liao, C.C. Chuang, C.W. Chang, Multifunctional PEGylated Albumin/IR-780/Iron Oxide Nanocomplexes for Cancer Photothermal Therapy and MR Imaging, Nanotheranostics 2 (2) (2018) 106–116, https://doi.org/10.7150/ntno.19379.
[62] I. Paraboschi, S. Turnock, G. Kramer-Marek, L. Musleh, M. Barisa, J. Anderson, et al., Near-InfraRed PhotoImmunoTherapy (NIR-PIT) for the local control of solid cancers: Challenges and potentials for human applications, Crit. Rev. Oncol. Hematol. 161 (2021 May) 103325, https://doi.org/10.1016/j.critrevonc.2021.103325.
[63] ClinicalTrials.gov ID NCT06699212. A Study of ASP-1929 Photoimmunotherapy in Combination With Pembrolizumab in First-line Treatment of Locoregional Recurrent Squamous Cell Carcinoma of the Head and Neck With No Distant Metastases (ECLIPSE). 2025.
[64] ClinicalTrials.gov ID NCT03769506. ASP-1929 Photoimmunotherapy (PIT) Study in Recurrent Head/ Neck Cancer for Patients Who Have Failed at Least Two Lines of Therapy. 2025.
[65] ClinicalTrials.gov I.D. NCT05265013. ASP-1929 Photoimmunotherapy Combined With Pembrolizumab in Patients With Recurrent Head and Neck Cancer, With or Without Metastases. 2024.
[66] J. Yuan, IR-780 Dye for Near-Infrared Fluorescence Imaging in Prostate Cancer, Med. Sci. Monit. 21 (2015) 511–517, https://doi.org/10.12659/MSM.892437.
[67] B.W. Pogue, E.L. Rosenthal, Review of successful pathways for regulatory approvals in open-field fluorescence-guided surgery, J. Biomed. Opt. 26 (03) (2021 Mar 13), https://doi.org/10.1117/1.JBO.26.3.030901.
[68] J. Lin, Q. Zhang, Reproducibility is a Process, Not. Achiev. Replica IR Reprod. Exp. (2020) 43–49, https://doi.org/10.1007/978-3-030-45442-5_6.
[69] A. Babu, S. Padmanaban, S. Chahal, A. Mohapatra, A. Sundaram, C.S. Cho, et al., Targeted nanoparticle delivery unleashes synergistic photothermal and immunotherapeutic effects against hepatocellular carcinoma, J. Nanobiotechnology 22 (1) (2024 Dec 1), https://doi.org/10.1186/s12951-024-03030-1.
[70] J. Kim, H. Cho, D.K. Lim, M.K. Joo, K. Kim, Perspectives for Improving the Tumor Targeting of Nanomedicine via the EPR Effect in Clinical Tumors, Int. J. Mol. Sci. 24 (12) (2023 Jun 13) 10082, https://doi.org/10.3390/ijms241210082.
[71] L. Chen, X. Deng, Q. Shen, M. Chen, C. Li, S. Wang, Novel Dual Strategy Based on EPR/AT for Optimizing Therapeutic Effect by Improving Drug Delivery System Physicochemical Properties and Regulating TME, Int. J. Nanomed. 21 (2026) 559763, https://doi.org/10.2147/IJN.S559763.
[72] H. Li, K. Wang, X. Yang, Y. Zhou, Q. Ping, D. Oupicky, et al., Dual-function nanostructured lipid carriers to deliver IR-780 for breast cancer treatment: Anti-metastatic and photothermal anti-tumor therapy, Acta Biomater. 53 (2017 Apr 15) 399–413, https://doi.org/10.1016/j.actbio.2017.01.070.
[73] Y. Kuang, K. Zhang, Y. Cao, X. Chen, K. Wang, M. Liu, et al., Hydrophobic IR-780 Dye Encapsulated in cRGD-Conjugated Solid Lipid Nanoparticles for NIR Imaging-Guided Photothermal Therapy, ACS Appl. Mater. Interfaces 9 (14) (2017 Apr 12) 12217–12226, https://doi.org/10.1021/acsami.6b16705.
[74] H. Yang, P. Zhao, Y. Zhou, Q. Li, W. Cai, Z. Zhao, et al., Preparation of multifunctional nanobubbles and their application in bimodal imaging and targeted combination therapy of early pancreatic cancer, Sci. Rep. 11 (1) (2021 Mar 18) 6254, https://doi.org/10.1038/s41598-021-82602-9.
[75] N. Zhang, Y. Tan, L. Yan, C. Zhang, M. Xu, H. Guo, et al., Modulation of tumor hypoxia by pH-responsive liposomes to inhibit mitochondrial respiration for enhancing sonodynamic therapy, Int. J. Nanomed. 15 (2020) 5687–5700, https://doi.org/10.2147/IJN.S256038.
[76] T. Lin, A. Yuan, X. Zhao, H. Lian, J. Zhuang, W. Chen, et al., Self-assembled tumor-targeting hyaluronic acid nanoparticles for photothermal ablation in orthotopic bladder cancer, Acta Biomater. 53 (2017 Apr 15) 427–438, https://doi.org/10.1016/j.actbio.2017.02.021.
[77] C. Yue, P. Liu, M. Zheng, P. Zhao, Y. Wang, Y. Ma, et al., IR-780 dye loaded tumor targeting theranostic nanoparticles for NIR imaging and photothermal therapy, Biomaterials 34 (28) (2013 Sep) 6853–6861, https://doi.org/10.1016/j.biomaterials.2013.05.071.
[78] T.N.H. Pham, P.T. Dang-Luong, H.P. Nguyen, L. Le-Tuan, X.T. Cao, T.D. Nguyen, et al., Therapeutic effect of F127-folate@PLGA/CHL/IR-780 nanoparticles on folate receptor-expressing cancer cells, Beilstein J. Nanotechnol. 15 (2024) 954–964, https://doi.org/10.3762/bjnano.15.78.
[79] S. Li, Q. Wang, Z. Jia, M. Da, J. Zhao, R. Yang, et al., Recent advances in glucose oxidase-based nanocarriers for tumor targeting therapy, Heliyon 9 (10) (2023 Oct) e20407, https://doi.org/10.1016/j.heliyon.2023.e20407.
[80] J. Song, H. Ye, S. Jiang, Y. Yang, X. Li, An acid response IR-780-based targeted nanoparticle for intraoperative near-infrared fluorescence imaging of ovarian cancer, Int. J. Nanomed. 17 (2022) 4961–4974, https://doi.org/10.2147/IJN.S375145.
[81] Z. Sheng, D. Hu, M. Zheng, P. Zhao, H. Liu, D. Gao, et al., Smart Human Serum Albumin-Indocyanine Green Nanoparticles Generated by Programmed Assembly for Dual-Modal Imaging-Guided Cancer Synergistic Phototherapy, ACS Nano 8 (12) (2014 Dec 23) 12310–12322, https://doi.org/10.1021/nn5062386.